Expertise
and insight
for the future

Anton Asplund

Design of a Four Wheel Drivetrain for an Electric Formula Student Vehicle

Metropolia University of Applied Sciences

Bachelor of Engineering

Mechanical Engineering – Machine Design

Bachelor's Thesis

28 September 2019

Author	Anton Asplund
Title	Design of a Four Wheel Drivetrain for an Electric Formula Student Vehicle
Number of Pages	57 pages + 2 appendices
Date	28 September 2019
Degree	Bachelor of Engineering
Degree Programme	Mechanical Engineering
Professional Major	Machine Design
Instructor	Pekka Hautala, Head of Competence Unit

This Bachelor's thesis describes the conceptual design of a drivetrain assembly consisting of a transmission and motor unit, to be used as a four-wheel drivetrain in the Formula Student Electric competition.

The conceptual design encompasses determining the load case and packaging constraints subjected to the drivetrain, choosing suitable motors and motor architecture through lap time simulation, and considering packaging constraints, as well as choosing the reduction ratio of the transmission through simulation.

As a result, the conceptual design of the transmission unit is described, along with choosing the type of gear train. In addition, the manufacturing method, material, and heat treatment for the gear set chosen are considered, after which the transmission concept design is elaborated. Finally, the concept design for the motor unit is also examined.

Keywords	Transmissions, Formula Student, Electric Vehicles, EV, Electric Drivetrains

Tekijä Otsikko Sivumäärä Aika	Anton Asplund Neliveto-voimansiirron konseptitason suunnittelu Formula Student Electric -autoon 57 sivua + 2 liitettä 28.9.2019
Tutkinto	Insinööri (AMK)
Tutkinto-ohjelma	Konetekniikka
Ammatillinen pääaine	Koneensuunnittelu
Ohjaaja	Osaamisaluepäällikkö Pekka Hautala

Insinöörityön tavoitteena oli sähköauton voimansiirron konseptin suunnittelu Formula Student Electric -autoon.

Suunnitteluun sisältyi voimansiirtoon kohdistuvien kuormien ja paketointirajoitteiden selvittäminen, moottorien ja moottoriasettelun määrittäminen kierrosaikasimulaatiota käyttäen, sekä alennusvaihteiston välityssuhteen määrittäminen simulaatiota käyttäen.

Vaihteiston konseptin kuvailuun kuului hammasvaihteen tyypin valinta, sekä myös hammasrattaiden valmistusmenetelmän, materiaalin ja lämpökäsittelyn valinta. Tämän jälkeen tarkasteltiin itse vaihteiston sekä moottoriyksikön konseptia.

Avainsanat	Vaihteisto, Formula Student, sähköautot, voimansiirto

I. Table of contents

I. Table of contents 4

II. Table of figures 6

III. List of Abbreviations 8

1 Introduction 1

2 Background 2

2.1 Formula Student 2
2.2 Metropolia Motorsport and earlier studies 3
2.3 Relevant work in literature 4

3 System boundary conditions 6

3.1 Load case 6
3.2 Packaging 7

4 Motor architecture 10

4.1 Performance comparison 10
4.2 Packaging 14
4.3 Reduction ratio 19

5 Conceptual design 22

5.1 Gear train 22
5.1.1 Initial gear train specifications 22
5.1.2 Manufacturing method 29
5.1.3 Material & heat treatment 31
5.2 Transmission 34
5.3 Motor unit 45
5.4 Drivetrain assembly 53

6 Conclusion and recommendations 57

7 List of references 58

8 Appendices 61

Appendix 1 – Vehicle speed vs. elapsed time, OptimumLap simulation, Autocross Spain 2018 61

Appendix 2 – Spreadsheet for mass of drivetrain assembly 62

II. Table of figures

Figure 2-1. CAD model of HPF019 motor package 3
Figure 2-2. CAD model of the motor unit situated in the chassis 4
Figure 3-1. CAD model of tubular frame (dark grey) and outboard suspension components (light gray) 8
Figure 3-2. Cross-section of the front wheel CAD assembly 9
Figure 4-1. CAD model of 1FE1041-6WM attached to front upright, isometric view 14
Figure 4-2. CAD model of 1FE1041-6WM attached to front upright, side view (from inboard) 15
Figure 4-3. CAD model of 1FE1041-6WM attached to rear upright, side view (from inboard) 16
Figure 4-4. CAD model of 1FE1051-4HC attached to front upright, isometric view 16
Figure 4-5. CAD model of 1FE1051-4HC attached to rear upright with rear wheel visible 17
Figure 4-6. CAD model of smaller 1FE1041-6WM motor unsprung at the front, and larger 1FE1051-4HC sprung at the rear 18
Figure 4-7. Normalised lap time vs. gear ratio for a gear ratio sweep study, 4x 1FE1041-6WM 20
Figure 4-8. Vehicle speed vs. elapsed distance, 75 m Acceleration, 4x 1FE1041-6WM 21
Figure 5-1. CAD model depicting limitation on gear ratio placed by 71814-B-TVH bearings, i=9.82 24
Figure 5-2. CAD model depicting the situation when an outboard 71815-B-TVH bearing is used, i=11.33 25
Figure 5-3. CAD model depicting upright assembly with larger 71815-B-TVH outboard wheel bearing 26
Figure 5-4. Comparison of lower wishbone mount bolt clearance, for current design (left) and proposed 71815-B-TVH design (right) 27
Figure 5-5. CAD model of situation when radial slots are cut in the outboard bearing shoulder, to accommodate larger planets, i=12.48 28
Figure 5-6. Wheel hub/planet carrier 35
Figure 5-7. Cross-section of wheel hub/planet carrier 36
Figure 5-8. Tool to extract planet pins using screws 38
Figure 5-9. Wheel hub assembly with bearing construction shown 39
Figure 5-10. Ring gear located in upright 41
Figure 5-11. Cross-section of transmission assembly in upright 42

Figure 5-12. Axial cross-section of transmission 44
Figure 5-13. Assembly and timing of gear train 45
Figure 5-14. Motor unit 47
Figure 5-15. Cross-section of motor unit 49
Figure 5-16. Cross-section of DE of motor unit 50
Figure 5-17. Cross-section of NDE of motor unit 52
Figure 5-18. Complete drivetrain 53
Figure 5-19. Cross-section of drivetrain 55

III. List of Abbreviations

4WD	Four wheel drive. All four wheels transfer tractive torque.
RWD	Rear wheel drive. Rear wheels transfer tractive torque.
FS	Formula Student. Engineering competition for University teams.
CAD	Computer aided design. Software that commonly is intended for 3D modelling and other engineering design related tasks.
WEDM	Wire electrical discharge machining. Machining process using electrical current passing through a fine wire to erode metallic materials.
DE	Driven end. Refers to the power output –side of a shaft.
NDE	Non-driven end. Refers to the opposite end of the power output –side.

1 Introduction

This Bachelor's thesis examines the design of a drivetrain for a Four-Wheel-Drive (4WD) Formula Student Electric car. The parent organisation behind this thesis is the Formula Student team of Metropolia University of Applied Sciences, Metropolia Motorsport. The team has used electrical Rear-Wheel-Drive (RWD) drivetrain units, driving each wheel with a separate motor, since switching to the electric discipline of the Formula Student competition. The team has considered the benefits of a 4WD drivetrain and as such has the desire of developing the current drivetrain unit to be 4WD, with each wheel driven with an individual motor.

The objective of this thesis is to consider the conceptual design for the drivetrain/motor and transmission -unit, more specifically the design of a unit which can later be further developed with detailed design. The concept design should include the choice of motors and their layout, transmission type and transmission ratio, as well as a 3D model of the suggested drivetrain system.

2 Background

2.1 Formula Student

Formula Student (FS) is an international engineering competition, where university students are tasked to conceptualize, design, and manufacture a small Formula-style race car to then compete against other universities' creations. Points are scored e.g. through the display of good engineering designs and practices, as well as naturally through the race car's on-track performance.

3 common FS disciplines exist; FS Electric, FS Internal Combustion, and FS Driverless, where the differences lie in the source of propulsion and for the driverless discipline, the existence of a human driver.

The on-track events – the dynamic events – can be identified as:

- Skid pad. A simple figure 8-shaped track to assess constant-radius cornering.
- Acceleration. 0-75 m acceleration.
- Autocross. 4 individual laps (not back-to-back) are driven on a track.
- Endurance. A track is driven X number of laps to equal approximately 22 km. A driver change takes place half way through.

In all these events, the rules laid out by the governing body limit the power drawn from the accumulator to 80 kW. The fastest Endurance time in the electric discipline of FS Germany 2018 was 1423 seconds (Formula Student Germany 2018) and considering that the accumulators can have energy capacities of approximately 25.3 MJ, this would result in an average power used - without considering regeneration - of approximately 17.8 kW. The real average power output is slightly lower than this value, though it still gives an indication of the low average power demands that the Endurance event places on the drivetrain – considering that this average power value is split between potentially 4 motors in a 4WD drivetrain. The Autocross and Acceleration events place higher power

demands on the drivetrain, but naturally the power is held for much shorter durations compared to the Endurance event, as the accumulator's energy level diminishes more quickly.

2.2 Metropolia Motorsport and earlier studies

Metropolia Motorsport, the parent team behind this thesis, has competed in FS since 2002 and has since 2013 competed in the FS Electric discipline. Since 2013, the electric cars developed have featured RWD drivetrains, and the teams' latest creation, the HPF019, features two Siemens 1FE1-family permanent magnet synchronous motors where each rear wheel is driven individually. The motor package for the HPF019 car, featuring two electric motor assemblies and two speed reduction transmissions, weighs approximately 46 kg, and including both drive shafts weighs approximately 47.5 kg. Figure 2-1 displays a Computer Aided Design (CAD) model of the motor package.

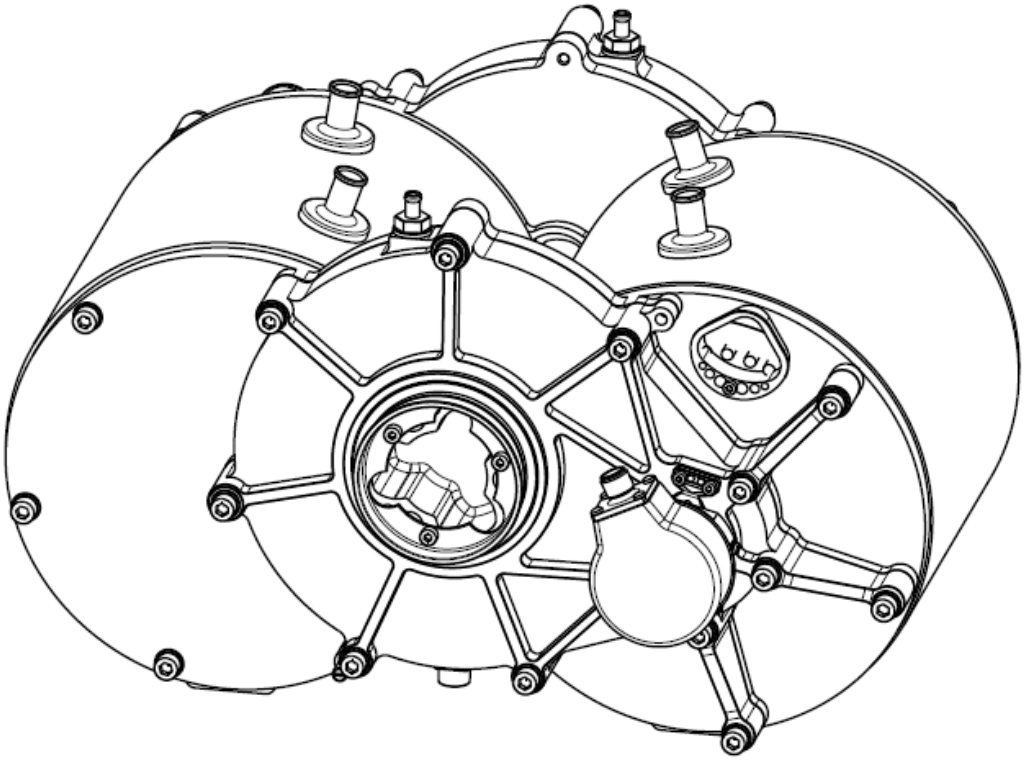

Figure 2-1. HPF019 motor package

The two motors are seen with their individual reduction transmissions symmetrically extending towards the middle. The position of the motor unit in the chassis is depicted

below in Figure 2-2, coloured light grey. The design of the first iteration of the motor package is described in a thesis authored by Lankila (2017).

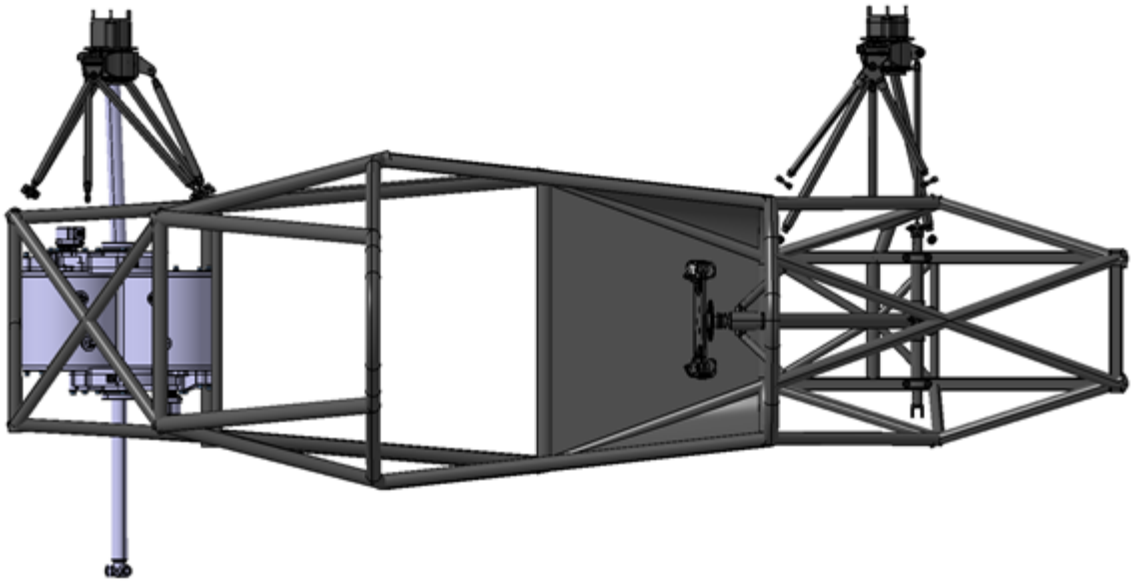

Figure 2-2. CAD model of the motor unit situated in the chassis

Hynninen (2017), a past member of the team, describes the conceptual design of a planetary geared upright-mounted drivetrain unit. Hynninen describes the general features and aspects of planetary gearing, the choice of the number of teeth for the transmission, gear ratio, efficiency calculations, as well as a strength analysis of the gears based on the SFS 4790 standard - which is in turn based on the ISO 6336 standard.

2.3 Relevant work in literature

Lynwander (1983) provides an insight into many gearing related topics, including a chapter on planetary gearing explaining their characteristics, gear ratio calculations, the concept of simultaneous / sequential meshing and hunting teeth, as well as conditions that ensure the possible assembly of the planetary gear sets.

Müller (1982) extensively covers a wide variety of epicyclic gear trains and describes aspects relating to various combinations of gear sets. Particularly the chapter ‘design hints’ discusses geometric conditions for the assembly of planetary transmissions, and load-sharing characteristics of the gear set. Simionescu (1998) derives general expressions for the assembly conditions of epicyclic gear trains.

Radzevich (2016) describes in depth various aspects relating to the design and manufacture of gearing, including e.g. design considerations, rating practice, material & heat treatment selection, manufacturing etc. Wire erosion, more specifically Wire Electrical Discharge Machining (WEDM) is covered by Uddeholm (2007), explaining the common effects that the WEDM process has on various steels in different conditions of heat treatment. Rao et al. (2015) displays the effect of various machining parameters on surface roughness values when using WEDM.

Planetary in-wheel gear trains are relatively common in the modern FS grid of electric cars, being employed by teams using motors mounted directly on the unsprung upright. A few publications have been made on this topic in the form of Bachelor's or Master's theses, where a few notable studies include the works of Beernaert (2016), Aune (2016), and Kucinski et al (2017). Danielsson et al. (2013) consider the characteristic differences between a 4WD and an RWD vehicle, as well as considering regenerative braking.

3 System boundary conditions

3.1 Load case

As described in Section 2.1, the dynamic events are divided into 4 categories. Both in the Acceleration and Autocross event, it is desirable to draw up to the full 80 kW from the accumulator as it will not run out of charge considering the low run times of both of these events. In the Endurance event, the power usage is limited to the battery capacity, and in the skid pad event, the power usage is set to a low level since a responsive throttle pedal is undesirable during steady state cornering.

A nominal life time of 40 hours can be identified as appropriate for the drivetrain. The total run time accumulated from 2 competitions, as seen from data gathered during driving, approximates to ~1 hour and 15 minutes of run time, meaning that a life time of 40 hours gives plenty of reserve for numerous competitions and a rigorous test season spanning at least 2 seasons. As this is the 1st attempt/iteration of a new drivetrain concept, and as a drivetrain component failure is generally disastrous for a competition weekend, a safety factor for fatigue of ~2 can be seen as appropriate – meaning that each critical component would last for 80 hours. Ideally, the bearings in the drivetrain would also last for the nominal system life time with a similar safety factor.

A classical stressing programme, consisting of using the estimated maximum load seen under operation, and extending it to the desired nominal life time of the system, can be seen as conservative. Load cases created from operational data are naturally more realistic, and useful when mass and system compactness is of priority.

The data gathered during the 2018 season from 2 competitions was collated into a spreadsheet showing the driver torque request (‘throttle’ pedal position), brake pressure to approximate brake pedal position, and car speed, as a function of time. As a load case involves knowing the percentage of time that a certain load and speed is held for, the data was sorted into a certain amount of cells that represent the number of times that the data rows fall under certain conditions. Table 3-1 illustrates the load case resulting from the data analysis.

Table 3-1. Load case showing the frequency of a certain power and a certain speed in each cell

Load case	Power (kW)						
Speed (km/h)	-20 - (-10)	-10 - 0	0-10	10-20	20-40	40-60	60-80
0-30	0.02%	3.29%	11.35%	0.19%	0.02%	0.00%	0.00%
30-60	0.96%	9.95%	26.05%	25.41%	2.07%	0.14%	0.00%
60-90	2.02%	4.87%	1.16%	4.30%	6.61%	0.82%	0.17%
90-120	0.10%	0.24%	0.003%	0.003%	0.02%	0.07%	0.16%

The load case is presented in the form of the entire car's behaviour, so that a motor load case using rev/min instead of km/h for speed and torque instead of power can be produced when the motor architecture is chosen. What can be seen from Table 3-1 is that the car spends more than half of the time drawing low power at speeds between 30-60 km/h, which is expected seeing as the average car speed during the Endurance event in one of the competitions was approximately 50.2 km/h. It is important that the occasional high power / low speed – i.e. high torque – cells as seen in Table 3-1 are taken into account into the stressing programme, as a momentary overload can produce a small crack which grows when the system is subjected to the expected low-torque loads, ultimately causing a fracture (Dowling 2013: 469).

The negative power –cells represent motor regenerative braking, with an arbitrary maximum regeneration power of 15 kW used for the load case that can be changed if desired. The effect on fatigue life that a load direction reversal such as regenerative braking might have should be taken into account in the stressing programme.

3.2 Packaging

Currently a motor unit is packaged into the chassis at the rear of the car. If separate motors at the front to drive the front wheels would be packaged into the chassis frame, significant modifications to the layout of the chassis would have to be made, especially considering that the rules laid out by Formula Student Germany (2019: 76) mention that electrical powertrain components have to be placed inside the rollover protection envelope. The rollover protection envelope can loosely be defined as the volume enclosed by the frame, shown in Figure 3-1.

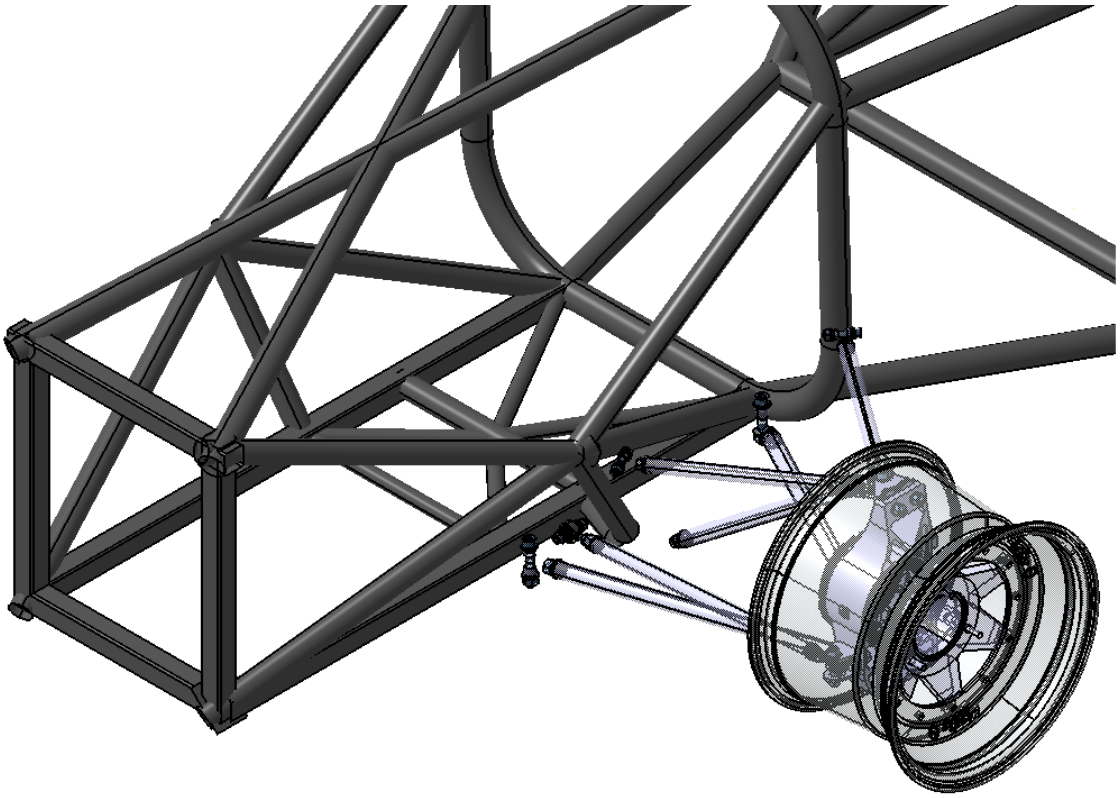

Figure 3-1. Model of tubular frame and outboard suspension components

The rules are relatively more lenient for ’outboard wheel motors’ (Formula Student Germany 2019: 76) i.e. in-wheel motors, however, a disadvantage of unsprung drivetrains is the effect it has on suspension performance, both in terms of unsprung mass as well as difficulties of packaging the suspension/steering arms around the motor to avoid clashing. The in-wheel drivetrain would also have to replace the wheel hub component and perform its functions satisfactorily. Figure 3-2 displays a cross section of the front wheel CAD assembly. A drivetrain packaged into the bore of the upright (where the outer rings of the wheel bearings are situated), must take into account e.g. the satisfactory functions of the wheel bearings, the preloading of the bearings, functioning as a brake disc mount and wheel centre mount, and naturally being sealed from the egress of oil were the drivetrain to be oil-lubricated.

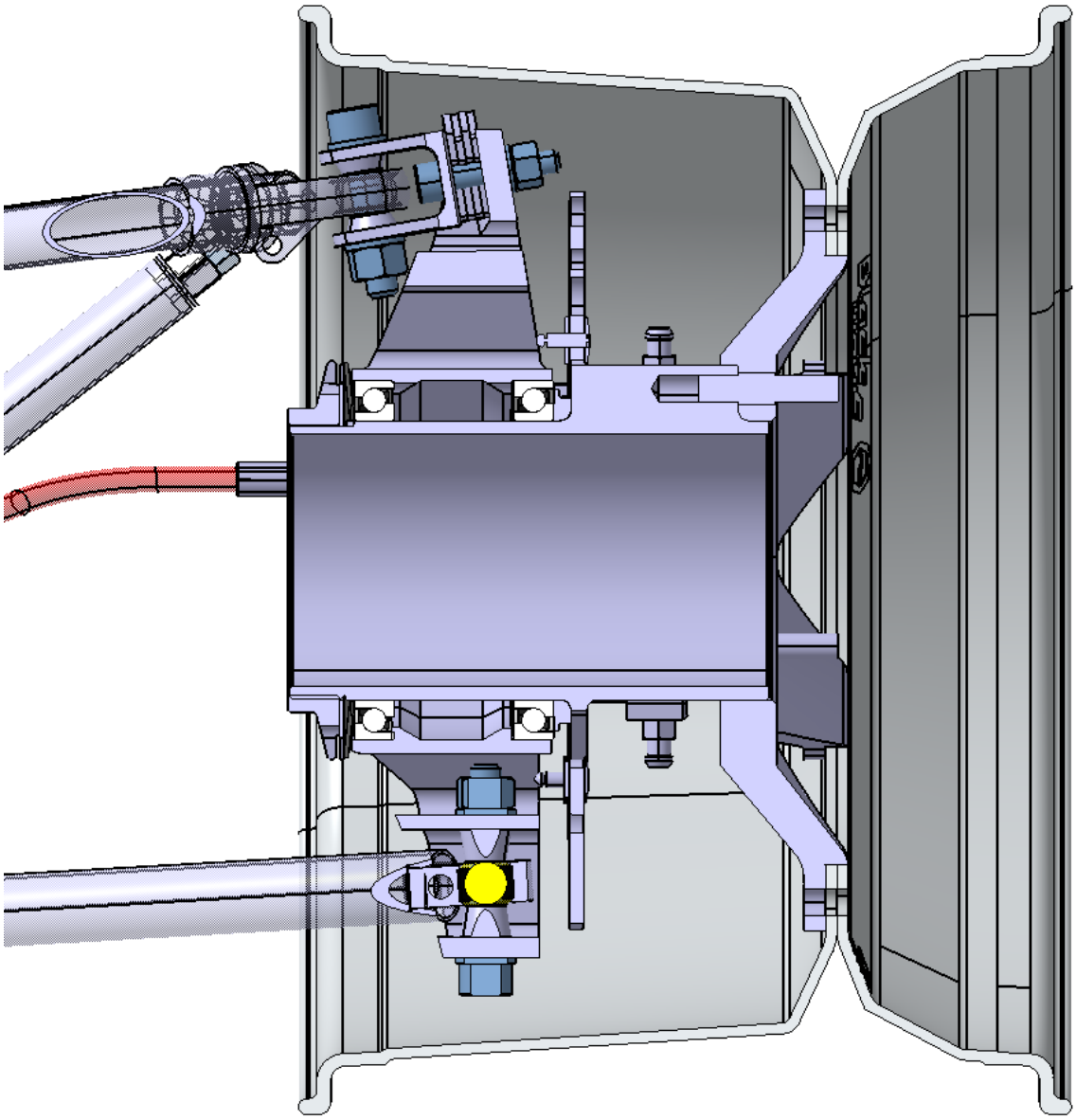

Figure 3-2. Cross-section of the front wheel CAD assembly

The wheel bearings currently employed are 90 mm in outer diameter and 70 mm in inner diameter. If larger wheel bearings would have to be specified, then packaging of the lower wishbone mount becomes more challenging with the current wheel size and mounting method. Any reduction in width between the two bearings would also be detrimental in terms of moment capacity. The current location of the brake disc mount is restricted by the width of the brake caliper, meaning that outboard movement of the brake mounting points is undesirable.

4 Motor architecture

4.1 Performance comparison

Siemens is one of the main sponsors of the FS team and supplies the project with inverters and motors. The team has used Siemens motors belonging to the 1FE1 product family since 2015, and the choice of motors for this drivetrain is similarly limited to the 1FE1 product family due to their most suitable performance and characteristics for the application in question. The 1FE1 motors are 'built-in' motors i.e. purely stators and rotors are supplied, meaning that the client is able to design bespoke casings and shafts around the components. The choice of motors for unsprung/in-wheel mounting was also limited to stators weighing less than 6 kg. Table 4-1 displays the product family narrowed down to possibly suitable unsprung motors.

Table 4-1. Comparison between various parameters of possibly suitable 1FE1 motors

Name (1FE..)	No. of poles	Stator + rotor mass (kg)	Rated power (kW)	Power density (kW/kg)	Rated current (A)	Rated speed (rpm)
1041-6WM	6	2.83	7.4	2.61	13	15,800
1051-6WK	6	5.20	8.3	1.60	15	8,000
1061-6WH	6	5.10	11.6	2.27	21	8,500
1051-4HC	4	4.10	12.6	3.07	25	24,000

Name (1FE..)	Maximum power (kW)	Maximum current (A)	Synchronous speed at 800 Hz (rpm)	Estimated gear ratio	Max power times 4 (kW)
1041-6WM	14.9	26	16,000	10.52	59.6
1051-6WK	14.2	40	16,000	5.33	57.0
1061-6WH	21.4	42	16,000	5.66	85.5
1051-4HC	27.6	50	24,000	15.99	110.6

When compared in a tabular form, it is immediately obvious that the weakest options of the 4 are the motors situated in the 2nd and 3rd row, featuring a relatively large mass paired with a low power density, possibly owing to their low rated speed.

The 1st option features a desirable mass, has a decent power density, and has a fair estimated reduction ratio, but produces relatively less power than the 4th option. The 4th option also features decent power density and produces a maximum power larger than

what the rules allow when multiplied by 4 (representing 4 individual motors), but is consequently slightly heavier than the 1st option. It is noteworthy, how the maximum inverter output frequency of 800 Hz limits any expeditions beyond the rated speed into the field weakening zone, which has to be taken into account when choosing reduction ratios.

To attempt at quantitatively deciding the motor layout, a coarse lap time simulation model was created using the software OptimumLap, to assess the lap time between configurations. OptimumLap only allows the input of basic parameters, though can still be used for crude comparisons and sensitivity studies such as these. The HPF019 vehicle was modelled with a theoretical constant-torque up until the maximum speed of the vehicle, to model a situation where the reduction ratio places the field weakening speed to coincide with the vehicle maximum speed seen under operation (~115 km/h).

OptimumLap features as default 8 different FS tracks that have been used in various official competitions in Europe and America. The Autocross data from FS Spain 2018 was also used to create a crude track for the model. A 75 m straight 'track' was also created to assess the Acceleration event. Different combinations of the 1st and 4th option of Table 4-1 were experimented with in addition to the base configurations. The results are shown in Table 4-2.

Table 4-2. Comparison of lap time results from OptimumLap model

	Single lap time (s)				
	Germany 2012	Nebraska 2013	Australia 2011	Michigan 2014	Nebraska 2012
HPF019 (2x 1082-6WP) (BASELINE)	87.76	56.85	55.02	63.73	68.71
HPF020-1 (2x 1041-6WM, 2x 1051-4HC)	82.37	54.06	53.16	60.96	66.38
HPF020-2 (4x 1041-6WM)	85.21	55.27	53.77	62.16	67.58
HPF020-3 (4x 1051-4HC)	81.04	53.54	52.88	60.46	65.70
HPF020-1-2 (2x 1041-6WM at 120 % max torque, 2x 1051-4HC)	81.94	53.87	53.06	60.78	66.17
HPF020-2-2 (4x 1041-6WM, 120 % max torque)	83.50	54.53	53.39	61.41	66.85

	Austria 2012	Germany 2010	Michigan 2012	Spain 2018	75m Straight	Avg. Difference (no Accel.)
HPF019 (2x 1082-6WP) (BASELINE)	54.56	51.44	50.16	79.03	4.69	
HPF020-1 (2x 1041-6WM, 2x 1051-4HC)	52.14	48.78	48.07	74.82	3.91	4.59%
HPF020-2 (4x 1041-6WM)	53.09	49.77	49.14	76.99	4.58	2.51%
HPF020-3 (4x 1051-4HC)	51.74	48.40	47.63	73.74	3.55	5.52%
HPF020-1-2 (2x 1041-6WM at 120 % max torq, 2x 1051-4HC)	52.00	48.65	47.92	74.47	3.80	4.90%
HPF020-2-2 (4x 1041-6WM, 120 % max torq)	52.48	49.13	48.47	75.73	4.19	3.79%

The current vehicle, HPF019, is shown at the top as a baseline. Three base configurations are shown after that – where the first configuration uses two of each motor option - with the last two configurations below the separating line representing base configurations that have been overloaded with 20 % more torque. The lap time results of 8 tracks + a 75 m straight are shown, with the average percentage difference from baseline for the 8 tracks shown on the bottom right.

It is visible how 4 of the more powerful motors (4th option in Table 4-1) produces the fastest lap time ('HPF020-3') as somewhat expected, and a combination using 2 of this 4th option and 2 of the 1st option in Table 4-1 produces the second best result ('HPF020-1') out of the three base configurations. The largest lap time out of the three is produced from the 'HPF020-2' configuration i.e. using 4 of the smaller motors. The result, however, is still more advantageous than the baseline configuration.

A hypothetical situation where the smaller motors are fed with 20% more maximum current is also entertained, representing both of the two lower rows ('HPF020-1-2' &

'HPF020-2-2'). The results expectedly show that the smaller motors produce a smaller lap time if momentarily overloaded for e.g. the Autocross and Acceleration event.

As mentioned earlier, a power restriction is placed on the car for the Endurance event, for the accumulator to last the entire event. A motor architecture with a nominal power equal to what is used in the Endurance event is therefore ideal as more powerful motors will result in 'dead weight' being carried around in the Endurance event. The FS competitions reward points using a different number of maximum points for each event, and different scaling coefficients for the equations by which points are calculated for each event. To explore the benefit of smaller motors for the Endurance event, an attempt was made to calculate the points difference between the configurations 'HPF020-1' and 'HPF020-2', shown in Table 4-3.

Table 4-3. Comparison of lap time results modified to represent event scoring

	Germany 2012	Michigan 2014
Endurance score		
HPF020-1 (2x 1041-6WM, 2x 1051-4HC)	127.3	185.0
HPF020-2 (4x 1041-6WM)	130.1	187.6
Autocross score		
HPF020-1 (2x 1041-6WM, 2x 1051-4HC)	58.2	8.8
HPF020-2 (4x 1041-6WM)	43.5	1.2
Acceleration score		
HPF020-1 (2x 1041-6WM, 2x 1051-4HC)	46.6	
HPF020-2 (4x 1041-6WM)	18.6	
Sum		
HPF020-1 (2x 1041-6WM, 2x 1051-4HC)	232.02	193.75
HPF020-2 (4x 1041-6WM)	192.2	188.9
Difference	**39.82**	**4.89**

What can be seen is that the advantage from a lighter car in the Endurance event is not as large as the advantage gained by having a more powerful car for the Autocross and Acceleration, which is then slightly heavier for the Endurance event. It is important to point out, however, that comparisons of this sort are imprecise at best, as the score depends on the elapsed time of the fastest car in that event. This can be seen in the large difference between the results of the Germany and Michigan –columns.

4.2 Packaging

The two motors were inserted into the HPF019 vehicle's CAD assembly for comparison. Depicted below in Figure 4-1 is the smaller 1FE1041-6WM motor directly attached to the front upright.

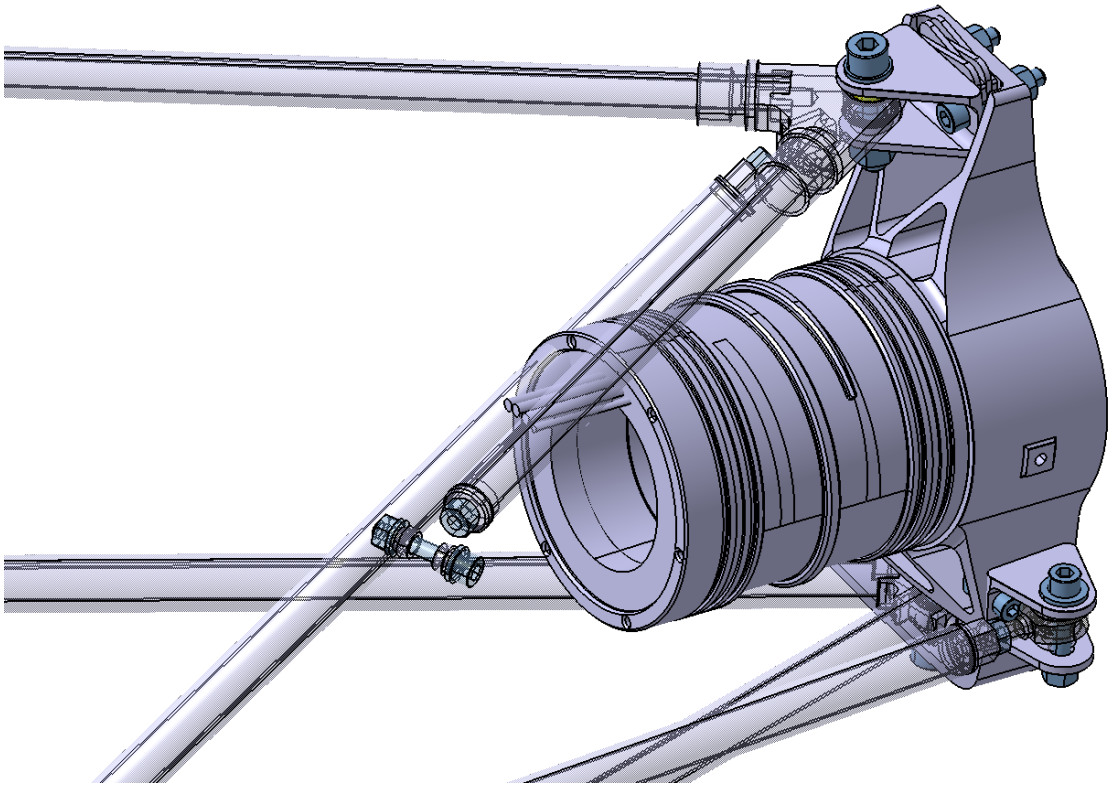

Figure 4-1. 1FE1041-6WM attached to front upright, isometric view

The motor is potentially well suited for an unsprung application, due to its relatively low mass and fair dimensions when compared with the upright in this fashion. What is visible is also the clashing of the pullrod suspension system used in the front suspension with the motor, depicted more clearly in Figure 4-2.

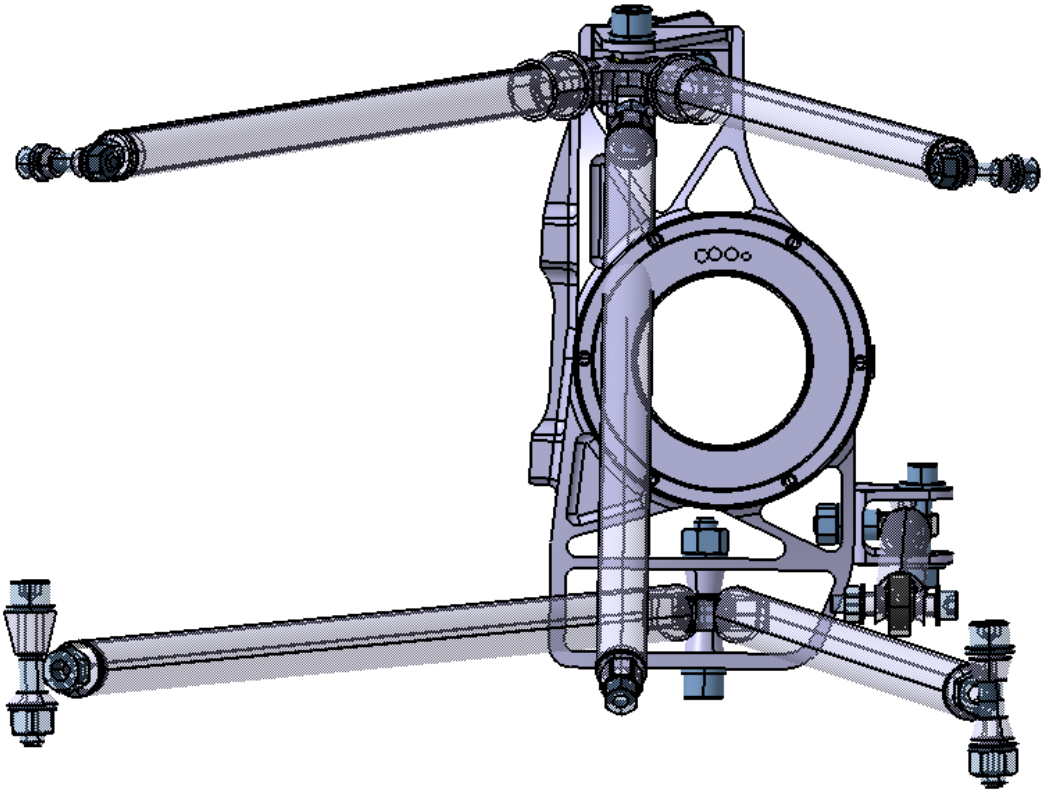

Figure 4-2. 1FE1041-6WM attached to front upright, side view (from inboard)

The possible implications of this is that the front suspension might have to be changed from a pullrod configuration to a pushrod configuration, by e.g. rotating the pullrod in Figure 4-2 by 180° i.e. still being attached on the upper wishbone and connected to a spring/damper situated at the upper levels of the frame instead of at the bottom levels. The dimensions of the motor seem to give fair clearance to the steering arm, though an in-depth kinematic analysis of the suspension geometry, which would be required if an unsprung motor system like this would be implemented, is beyond the scope of this thesis, meaning that no quantitative statements in this regard can be made here.

The situation is similar if the motor is compared with the rear upright, as shown in Figure 4-3. The rear suspension uses a pushrod configuration, which would potentially be required to connect to the upper wishbone instead of near the lower wishbone as shown.

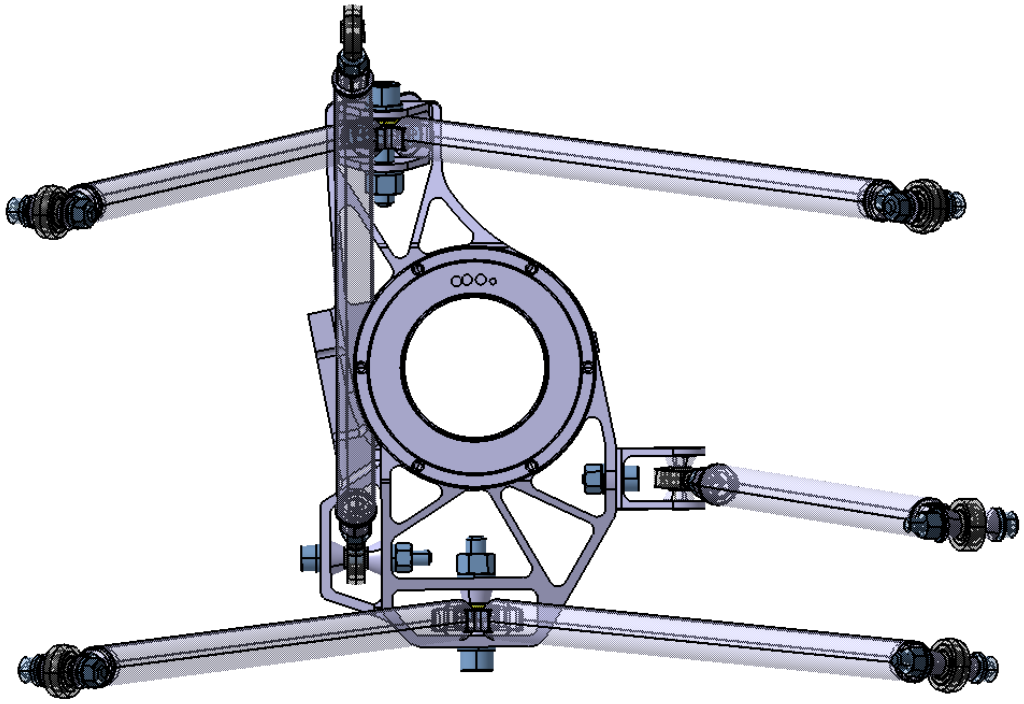

Figure 4-3. 1FE1041-6WM attached to rear upright, side view (from inboard)

The situation is different when comparing the larger 1FE1051-4HC motor (4th option in Table 4-1) with the upright, depicted below in Figure 4-4.

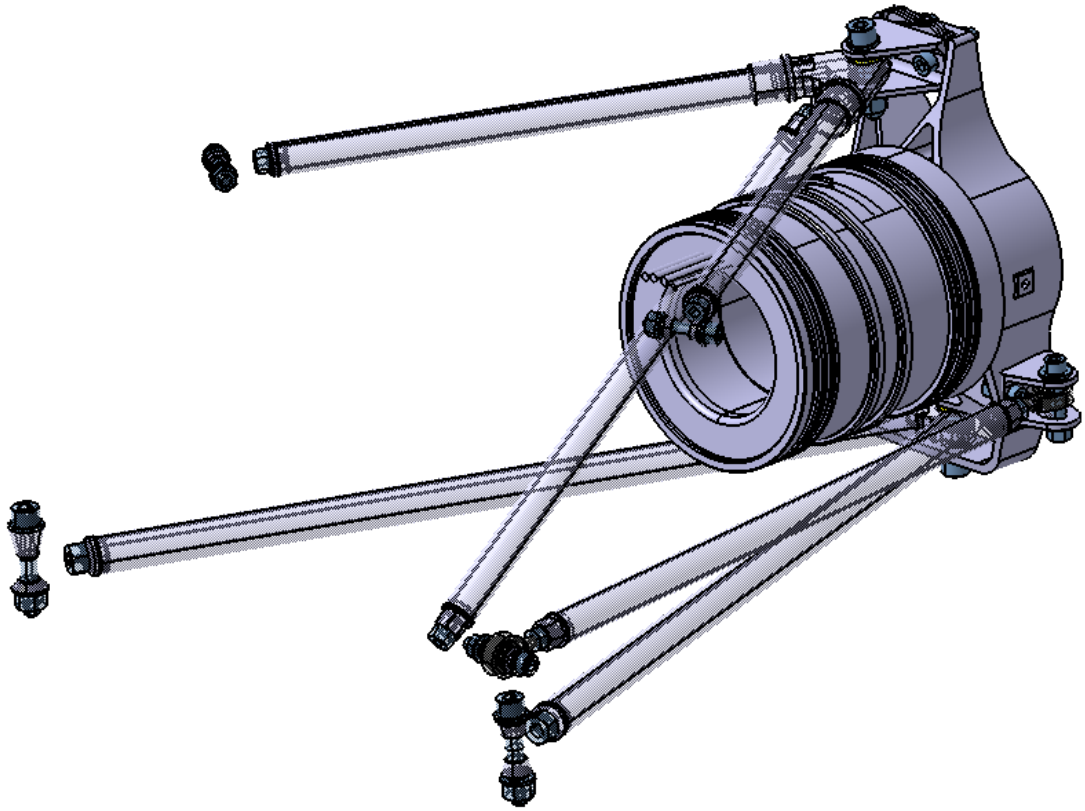

Figure 4-4. 1FE1051-4HC attached to front upright, isometric view

In comparison to the smaller motor, the larger motor looks almost prohibitively large, and accompanied with the relatively larger mass, could potentially turn out to be too eager a choice in view of the fact that this is the 1st iteration of such a system, and any possible problems that might appear in the later stages of the design process, such as suspension clashes, are then very costly to correct, time wise. The motor is shown connected to the rear upright with the rear wheel visible in Figure 4-5.

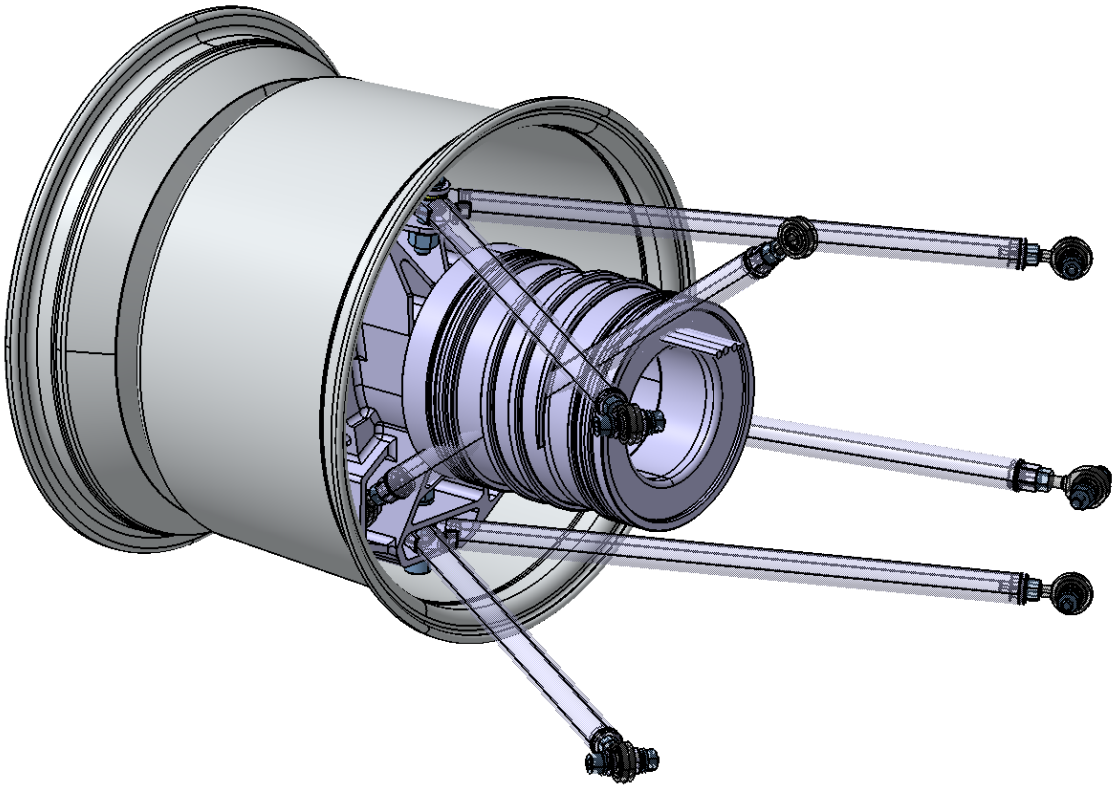

Figure 4-5. 1FE1051-4HC attached to rear upright with rear wheel visible

A potential compromise is using the smaller motors unsprung at the front, and the larger motors, sprung, packaged into the rear of the chassis. This suggestion is depicted below in Figure 4-6.

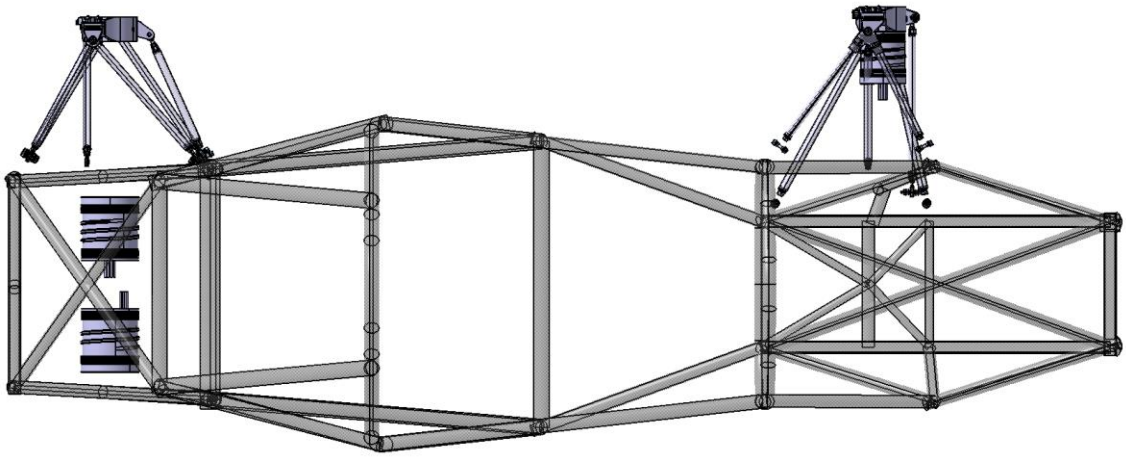

Figure 4-6. Smaller 1FE1041-6WM motor unsprung at the front, and larger 1FE1051-4HC sprung at the rear

The rules, as mentioned earlier, restrict any part of the drivetrain from extending beyond the rollover protection envelope i.e. frame. Packaging the two larger motors axially next to each other might be problematic in this aspect, as each of the motors require the packaging of a transmission at the drive end, and an encoder at the non-drive end, both required to stay inside the frame. The motors could potentially be physically separated from each other at the non-drive end, simplifying the casing construction and making assembly easier. As the motors are not 'stressed' chassis components[1], the stiffness of the motor unit is less crucial, allowing them to be physically separated.

Out of the options presented, the combination of the two motors as shown in Figure 4-6 seems like the best option. The second best option would be using 4 of the smaller motors, potentially all of them as unsprung since the resource savings from using the same drivetrain at the front and rear wheels can be significant. Another benefit from this is also that the rear compartment of the frame can be entirely removed, reducing mass, and reducing the polar moment of inertia of the car.

From a project management point of view, the focus will firstly be placed on developing the front in-wheel drivetrain, and secondly on developing the rear sprung drivetrain after a front wheel drivetrain has been designed. This priority ordering has a larger chance of producing a successful project, with a drivetrain that is still more advantageous than the

[1] A 'stressed' powertrain in chassis design – common in internal combustion race cars - refers to deliberately replacing part of the frame with the powertrain, i.e. mounting suspension hard-points, rear wing etc... onto the powertrain casing instead of onto the separate frame.

current drivetrain, instead of attempting at attacking two designs at the same time with a larger risk at not meeting project objectives.

4.3 Reduction ratio

As visible from Table 4-1 (’Synchronous speed’), the 1041-6WM motor speed is capped to the value of the synchronous speed, which in this case coincides closely with the start of the field weakening zone (rated speed). The reduction ratio can then simply be chosen as to have the motor operate at its capped speed at the end of the 75 m acceleration straight – where the car reaches around 113...118 km/h. It can be experimented, however, with using a higher ratio than this, meaning that the car would drive with a constant speed for some distance at the end of the 75 m straight.

OptimumLap was again used to experiment with changing the reduction ratio. The same tracks were used with a sweep across ratios 10...15 for the situation where 4 of the smaller 1041-6WM motors are used. The baseline ratio to compare results with was approximately 10.66, which would place the maximum motor speed at approximately 115 km/h. Figure 4-7 displays the results of the experiment.

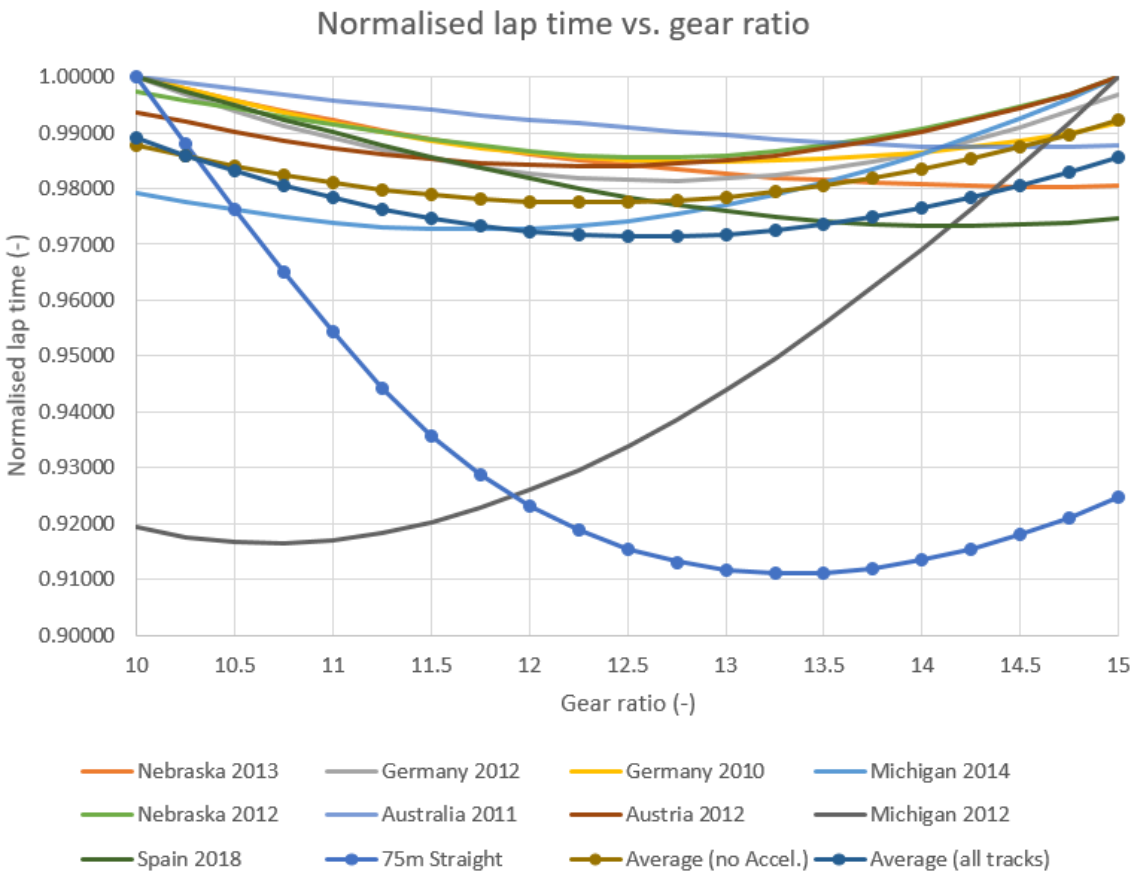

Figure 4-7. Normalised lap time vs. gear ratio for a gear ratio sweep study, 4x 1FE1041-6WM

The beaded traces represent the most interesting results. When taking the average of the results from the track events and excluding the Acceleration event, the resulting 'optimal' reduction ratio is approximately 12.25 instead of the initial 10.66. Including the Acceleration event shifts the average reduction ratio slightly higher to approximately 12.50. When plotting the vehicle speed vs. elapsed distance for the Acceleration event with a few select ratios, the results are as shown in Figure 4-8.

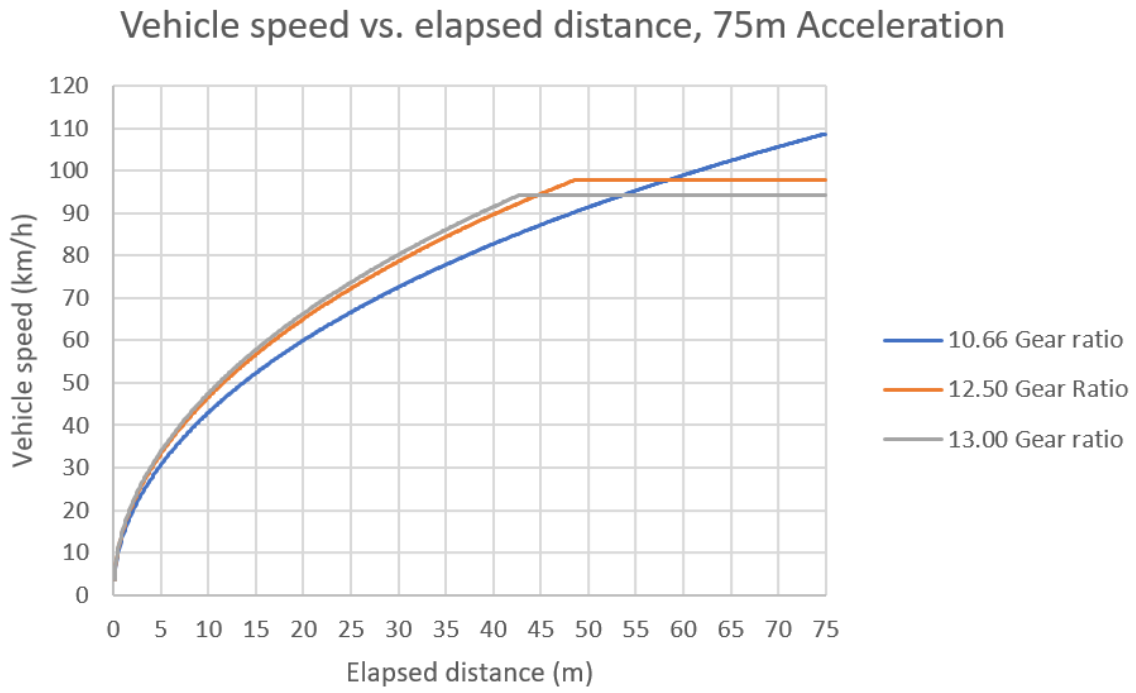

Figure 4-8. Vehicle speed vs. elapsed distance, 75 m Acceleration, 4x 1FE1041-6WM

As can be seen, the vehicle would then reach the maximum speed at approximately 100 km/h when using a reduction ratio of 12.50. Analysing the vehicle speed vs. elapsed time for the simulated 2018 Spain Autocross shows that the vehicle clearly peaks in speed only at one point during the lap when using a ratio of 12.50 (Appendix 1). Data from the actual Autocross event in Spain 2018 shows that the HPF019 vehicle saw a maximum speed of 92.8 km/h in the fastest lap performed. This ratio of 12.50 will be set as an initial target.

5 Conceptual design

5.1 Gear train

5.1.1 Initial gear train specifications

To achieve a reduction ratio of 12.5 in a compact space, the transmission would realistically have to feature a gear train. A spur gear system would require offsetting the motor axis, which is undesirable from a suspension kinematics point of view, and would additionally require a large amount of space to achieve such high reduction ratios. A planetary gear train seems to be the most feasible option for the transmission. Three planets also seem to be the most advantageous number of planets, as an initial choice, to achieve theoretical equalisation of the radial loads that result from meshing.

The unique situation of an in-wheel planetary gear train creates unusual constraints. Ideally the transmission is situated inside of the wheel hub to reduce the axial space, and as described in Section 3.2, must then fulfil the functions of a wheel hub. If the ring gear is locked in the gear train and the planetary carrier is the output – to achieve the largest possible reduction ratio – then the carrier needs to potentially incorporate the wheel bearings into its construction. The implications of this are that a two-stage planetary gear train, with the ring gear locked in both stages, would need to allow the relative rotation of both carriers in each of the stages, while being able to transfer axial loads resulting from cornering, through both of the carriers and into the inboard wheel bearing. This could potentially create a relatively complicated structure. When cornering in the opposite direction, the axial load only needs to travel to the outboard wheel bearing to then reach the supporting upright. A single stage gear set is then more advantageous for packaging, however the upper limit for reduction ratios of a single stage gear set is at 10:1 (Lynwander 1983), as either the sun gear becomes very small in size and stress-limited or then the planets collide with each other.

A compound planetary gear set apparently gives good results for gear ratios between 10:1 and 16:1 (Lynwander 1983), and will be explored initially. The carrier can then potentially be supported by the two wheel bearings more easily. The current uprights with their 71814-B-TVH wheel bearings were used for reference to explore concepts. To attempt at achieving a small gear train, a module of 0.5 mm was initially used to explore

the gear sets possible, as a 0.75 mm module already results in relatively large gear sets with the desired ratio. Another benefit of a small module is the increase in efficiency it provides as pitch line speeds decrease. The axial assembly of the planets is also desirable to attempt at simplifying the carrier construction and assembly procedure – as the entire gear 'cassette' can be assembled or removed from the upright as a complete unit.

The sun gear can be placed on the inboard side of the upright, but a more flexible sun gear shaft can be beneficial in terms of the load sharing capability between the three planets, as long as the critical speed of the shaft does not cause problems.

It became obvious already at the early stages of the concept design process that the 71814-B-TVH bearings place restrictions on the size of the 1st planet gears – if axial assembly is to be fulfilled. Figure 5-1 depicts the situation when a gear set with the ratio of ~9.82 is able to be axially assembled into the upright, where the addenda of the 1st planet gears are able to clear the bearing shoulder of the outboard wheel bearing. Even with an already small module of 0.5 mm, the reduction ratio achievable with the current methods and bearings suggested is unsatisfactory.

It is also visible in Figure 5-1 that if radial assembly of the planets is instead acceptable, then a radial slot would have to be cut into the upright behind the outboard bearing, to fit the 1st planet gears if they were to be made larger in size.

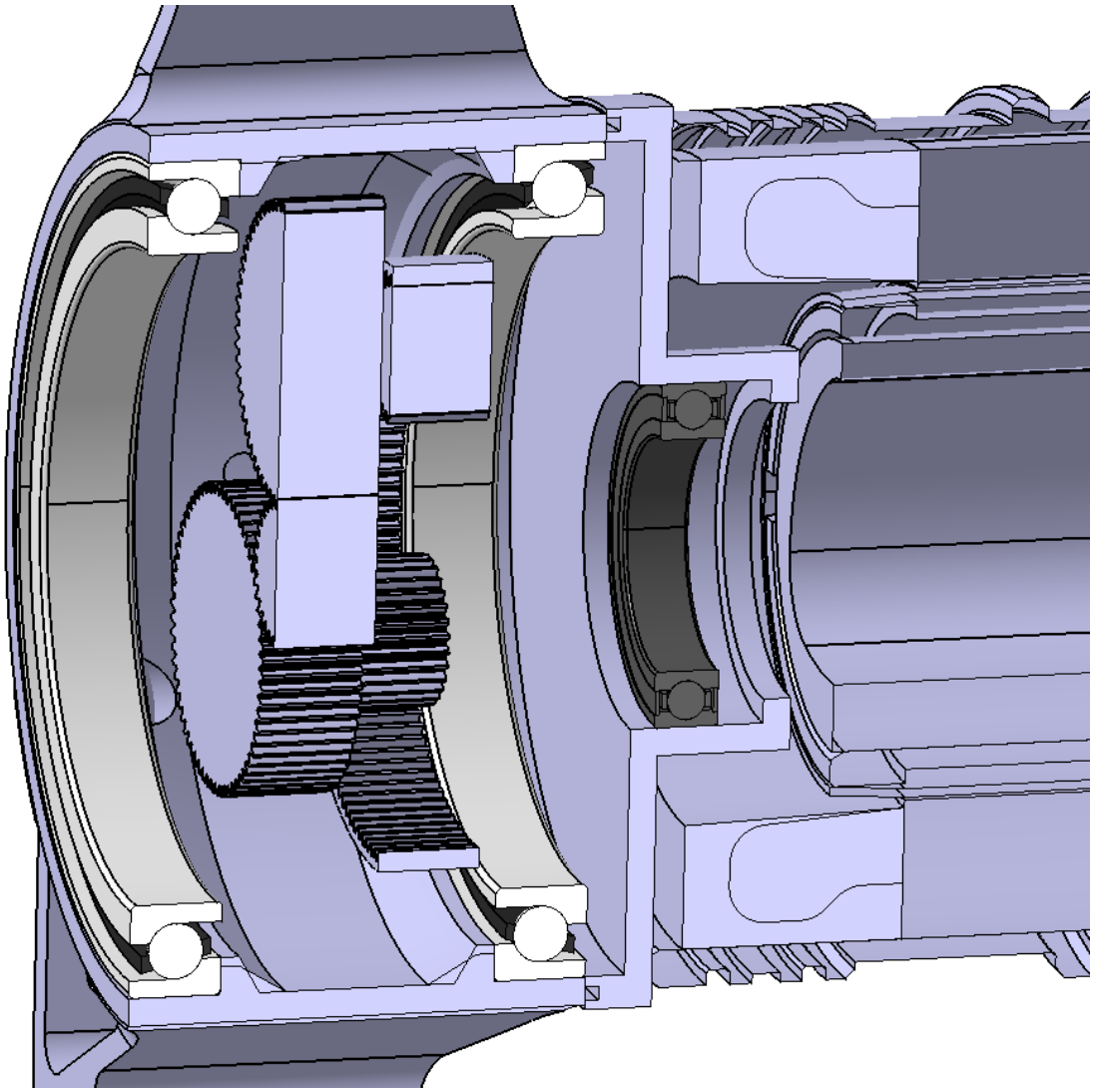

Figure 5-1. CAD model depicting limitation on gear ratio placed by 71814-B-TVH bearings, i=9.82

If the outboard 71814-B-TVH bearing is substituted for a one step larger 71815-B-TVH bearing, then a ~11.33 ratio gear train could be packaged into the upright, where the addenda of the 1st planet gears inscribe a circle very close to the outboard bearing shoulder. This situation is depicted in Figure 5-2.

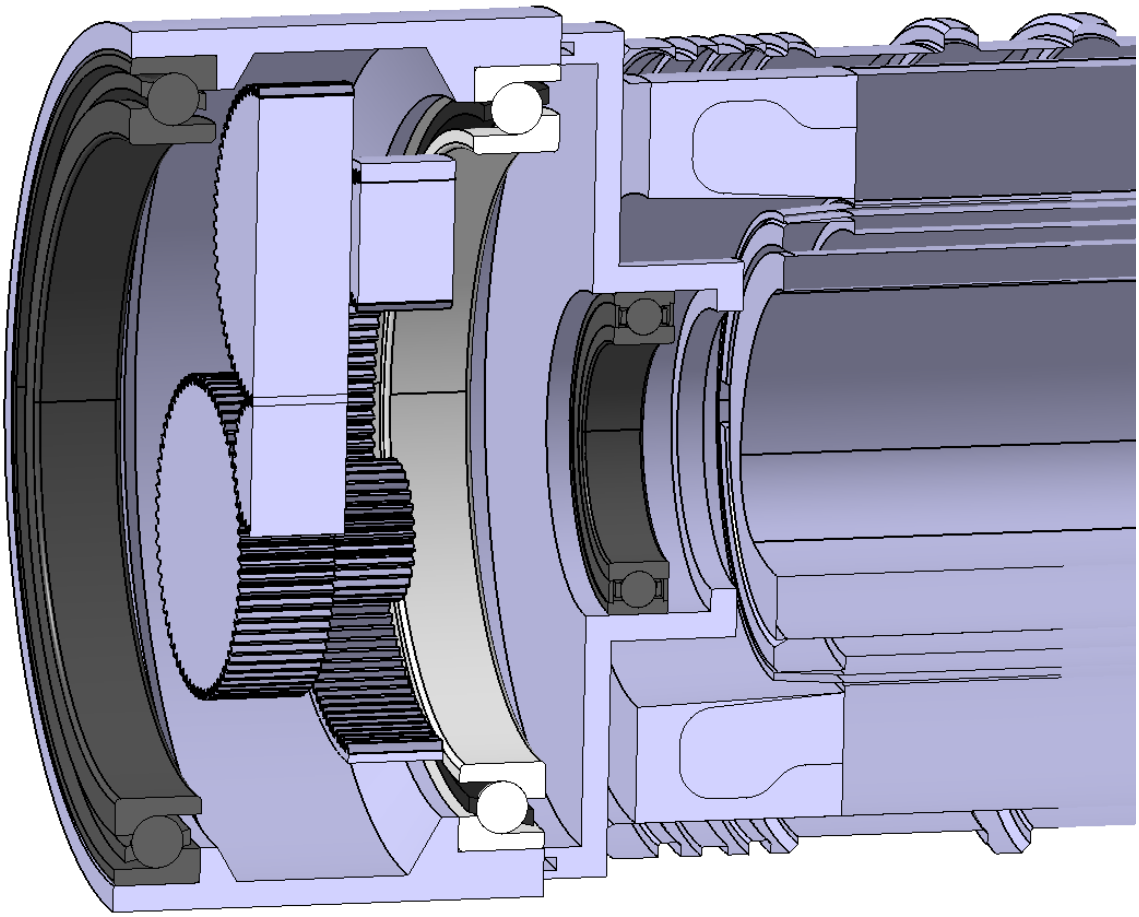

Figure 5-2. CAD model depicting the situation when an outboard 71815-B-TVH bearing is used, i=11.33

The most important implications of a larger outboard wheel bearing is the effect it has on suspension packaging. The assembly depicted above in Figure 5-2 is shown inserted into the current upright assembly for comparison below in Figure 5-3.

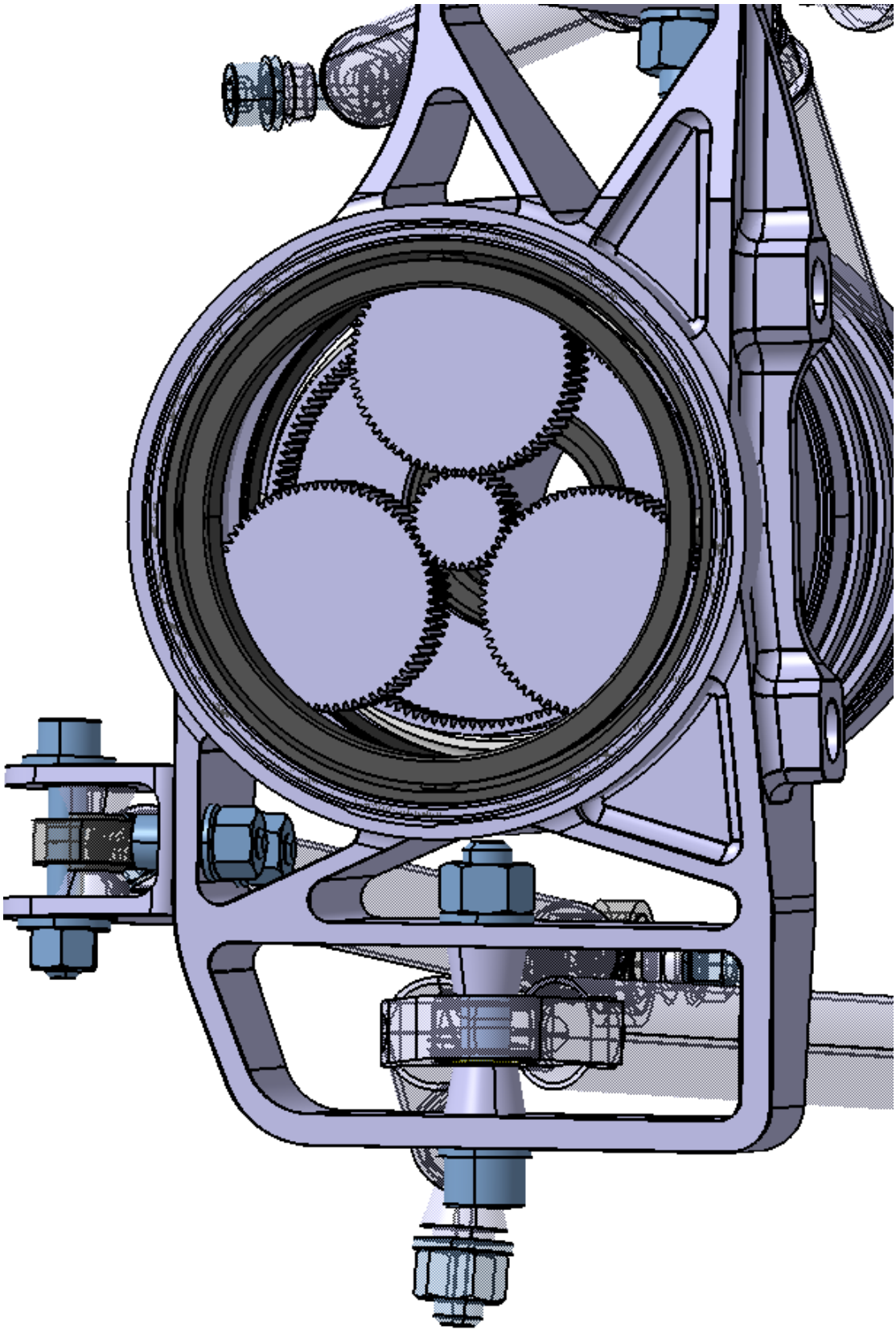

Figure 5-3. HPF019 upright assembly with larger 71815-B-TVH outboard wheel bearing

The outer diameter of the bearing bore clears the brake caliper attachment on the right-hand side, and barely clears the bolt for the lower wishbone mount, however the situation is not ideal from an assembly point of view. Figure 5-4 displays the clearance available for the standard M8x50 bolt used in the lower wishbone mount, for the current design and proposed design above. A small cutout can potentially be provided in the upright at this particular location to give slightly more clearance for the bolt.

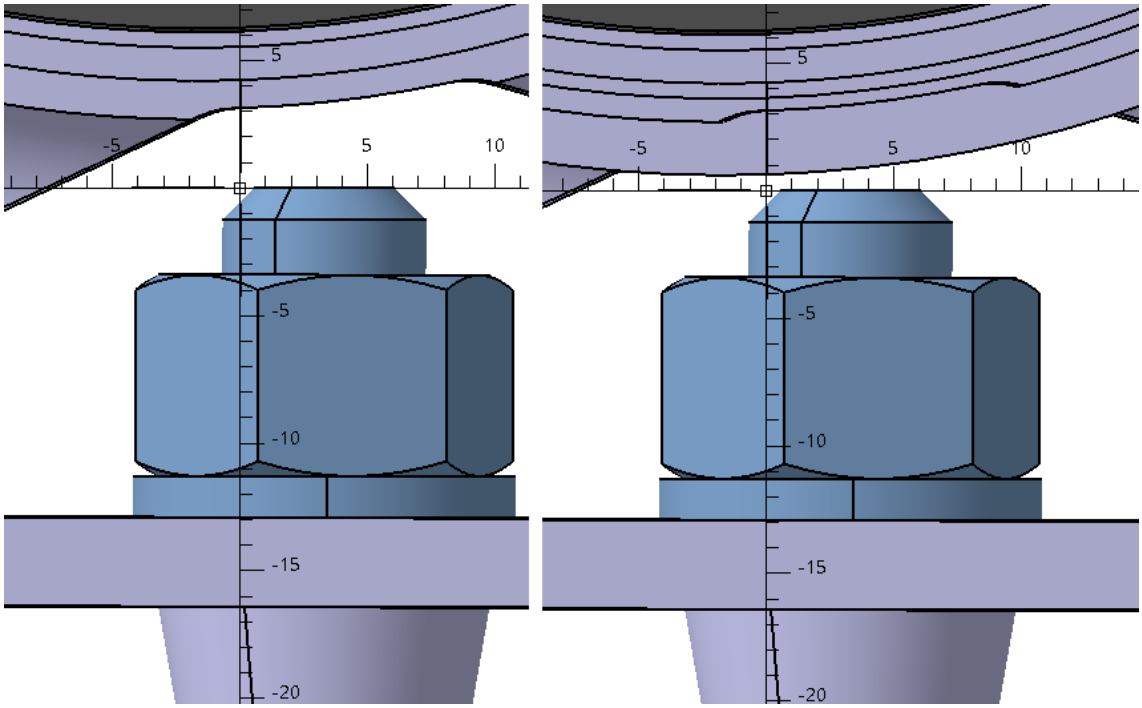

Figure 5-4. Comparison of lower wishbone mount bolt clearance, for current design (left) and proposed 71815-B-TVH design (right)

A reduction ratio of 11.33 is more advantageous than the previously depicted 9.82, though is still not ideal. To achieve a ratio closer to the target 12.5, radial slots can be cut into the upright outboard bearing shoulder, to allow larger diameter 1st stage planet gears to be axially assembled. Figure 5-5 displays the situation when a gear set featuring the reduction ratio of 12.48 is used.

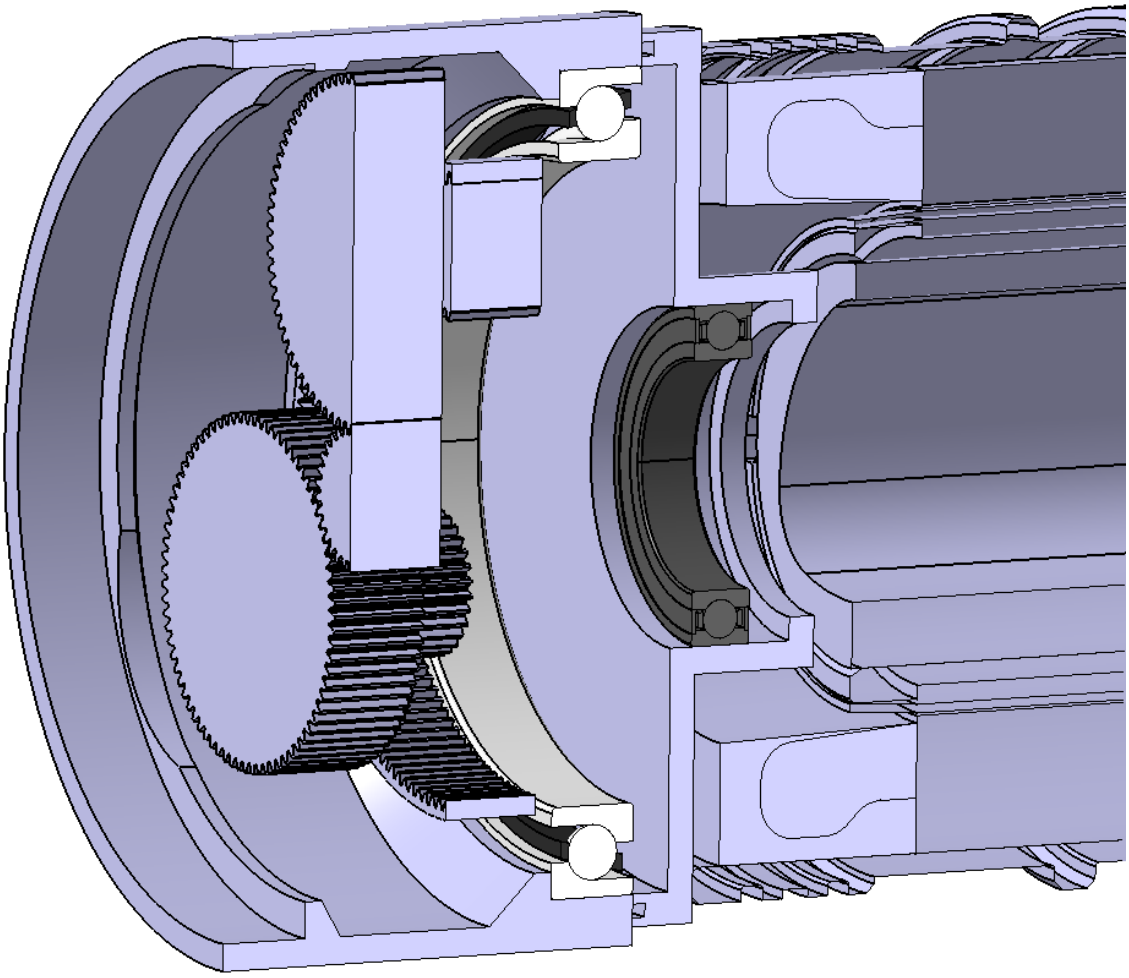

Figure 5-5. CAD model of situation when radial slots are cut in the outboard bearing shoulder, to accommodate larger planets, i=12.48

The number of teeth in the gear set were then examined for the assembly of the compound planetary transmission, to which Müller (1982: 320) gives a condition that must produce an integer in order for the transmission to be assembleable using even spacing of the planets;

$$\frac{|z_{p1} * z_{ring}| - |z_{sun} * z_{p2}|}{n_{planets} * GCD_{zp1,zp2}} = integer$$

where:

- z_{p1}, z_{ring}, z_{sun}, z_{p2} are the number of teeth of the first planet gears, ring gear, sun gear, and secondary planetary gears, respectively.
- $n_{planets}$ is the number of planets (3)
- $GCD_{zp1,zp2}$ is the greatest common divisor of z_{p1} and z_{p2}

Lynwander (1983: 316) similarly gives a condition for compound planetary gear sets which must produce an integer in order for the transmission to be assembleable:

$$\frac{z_{ring} + \frac{z_{sun} * z_{p2}}{z_{p1}}}{n_{planets}} + \left(H_{p1} - H_s\right) * \frac{z_{p2}}{z_{p1}} = integer$$

where:

- Integers are substituted for (H_{p1} - H_s)

The gear set was also examined for the hunting teeth situation using the 'Kish method' (Kish 1997), sequential meshing of the sun gear and primary planet gears (Lynwander 1983: 318), and that the number of teeth on the ring gear is divisible by the number of planets, to ensure that all planetary gear pairs can be manufactured identically, instead of requiring that each planet pair must feature unique angular 'timing' of the teeth (Aune 2016: 106).

After these checks, the total reduction ratio reduced to 11.26. Table 5-1 displays the number of teeth suggested.

Table 5-1. Number of teeth of initial gear set (not validated for strength), i=11.26

	Sun	*Planet 1*	*Planet 2*	*Ring*
No. of teeth	29	76	36	-141

The module for all of the gears are set as 0.5 mm as an initial value. The maximum width of the gears would ideally be approx. 12 mm wide. The widths and modules will invariably only be precisely defined when the complete stressing programme is carried out and additionally as e.g. the pinion of each mesh is made slightly wider to accommodate for axial tolerances that build up in the assembly. The choice of profile shift coefficients and tooth form modification factors are also to be considered in conjunction with the stressing programme.

5.1.2 Manufacturing method

Gear production is generally fairly costly, especially small batch production such as for FS applications. Traditional gear hobbing, hardening, and grinding has been employed in the past for previous drivetrain systems such as the one depicted in Figure 2-1, where

the single-stage spur gear pair employed featured a module of 2.25 mm. The production of ring gears for epicyclic gearboxes are more costly, especially at the small considered module of 0.5 mm.

Machining (e.g. turning) will be used to manufacture the gear blanks, after which the involute geometries could be made using a Wire Electrical Discharge Machining (WEDM) process. The characteristics of the WEDM process allow it to machine involute geometries (external/internal), and other geometrical connections (e.g. involute splines, polygon fits) to a potentially acceptable level of precision, without the need of several different cutting tools. WEDM can also cut the gear blanks in the hardened condition, avoiding the distortions associated with hardening gears that are already finish-machined. Internal stresses released during the WEDM process might however distort the part, and the gear blank should be as close to net shape as feasible to attempt at reducing this distortion. The surface finish on WEDM cut parts can be good, potentially reaching values of 0.2 - 0.3 µm, according to Uddeholm (2007). The thickness of the locally hardened re-melted white layer inherent in Electrical Discharge Machining processes is also fairly thin in the WEDM process, approximately 2 - 4 µm thick, with negligible influence on mechanical properties (Uddeholm 2007). All of these characteristics combined make the WEDM process seem like an attractive option, and will be specified for the gears initially.

Individual transmissions could be assembled as whole units which can be conveniently swapped out as complete packages if needed, reducing downtime. To attempt at alleviating the impact of e.g. manufacturing tolerances, these individually assembled transmission units can also be ran in using a lapping compound prior to operation.

5.1.3 Material & heat treatment

Table 5-2. Typical mechanical properties of potential gear materials

Typical mechanical properties of potential gear materials

Supplier	*Designation*	*Heat treat process*	*Comments*
Ovako	34CrNiMo6	Q + T	Quenching & tempering steel
Ovako	IQ-steel X800 (100Cr6)	Q + T	Through hardening steel
Ovako	IQ-steel X600	Q + T	Through hardening air-hardening steel
Ovako	IQ-steel X300 (42NiSiCrMo8-7-3F)	Q + T	Quenching & tempering steel
Ovako	IQ-steel X200	Q + T + gas nitriding	Strength values= core strength
Aubert & Duval	ML340 (X23NiCoCrMoAl13-6-3)	Aging 495°C/10 hrs	Duplex hardening type steel (high cost?)
Aubert & Duval	NC310YW (40SiNiCrMoV10)	Q + sub-zero treat + 2xT	High cost
SSAB	Toolox 44	Gas nitriding (supplied as Q+ T)	Strength values= core strength

Supplier	*Designation*	*Surface hardness*	$R_{p0.2}$ *(MPa)*	R_{UTS} *(MPa)*	*Elongation* A_5 *(%)*
Ovako	34CrNiMo6	50 HRC	1200	1500	7 %
Ovako	IQ-steel X800 (100Cr6)	61 HRC	1700	2300	2 %
Ovako	IQ-steel X600	61 HRC	1700	2300	2 %
Ovako	IQ-steel X300 (42NiSiCrMo8-7-3F)	53 HRC	1550	2100	8 %
Ovako	IQ-steel X200	840 HV (~65 HRC)	650	730	20 %
Aubert & Duval	ML340 (X23NiCoCrMoAl13-6-3)	-	1900	2220	10% (5d)
Aubert & Duval	NC310YW (40SiNiCrMoV10)	-	1790	2150	9% (5d)
SSAB	Toolox 44	825 HV (~65 HRC)	1300	1450	13 %

Table 5-2 displays a table of potential materials for the gear wheels along with their typical mechanical properties. Ovako has been a trusted partner of the parent organisation for many seasons, and their steels are preferred firstly. The traditional 34CrNiMo6 offers good strength when quenched & tempered and when a hardness of 50 HRC is specified. Both of the “IQ-steel X800” and “IQ-steel X600” steels offer excellent strengths, and excellent hardness values, however their elongation of 2 % is unacceptable. The “X200” when gas nitrided has good surface hardness however features fairly low core strength values, which could unfavourably cause the failure mode of the gears to be in bending. The “X300” provides a middle ground between the 3 steels, and seems to balance strength with elongation well.

Aubert & Duval offers materials intended for highly demanding applications. Two of their steels are shown in the table, and what is noticeable is their high strength paired with good elongation. The prices however may be too prohibitive, and Aune (2016: 74) reports “a cost difference of 1000 % compared to the baseline steel” (baseline: 1.6587 / 18CrNiMo7-6) for the NC310YW steel. Toolox 44 as supplied by SSAB has been very successfully used in the past for highly stressed drivetrain components (e.g. shafts), and

might be an alternative for the gears especially when nitrided, featuring higher core elongation than the Ovako X300 alternative and excellent nitrided surface hardness. The core surface hardness is approximately 45 HRC as supplied.

Table 5-3. Comparison of characteristics between various heat treatment processes

Comparison of characteristics between various heat treatment processes

Process	*Comments*	*Torque capacity (1-5)*	*Surface hardness (1-5)*	*Distortion*
Gas nitriding	WEDM cut before HT process	2	5	Low
Ion nitriding	WEDM cut before HT process	3	5	Low
Carburising & quenching	WEDM cut before HT process	5	3	High
Carbonitriding	WEDM cut before HT process	4	4	Medium
Through hardening (Q+T)	WEDM cut after HT process	1	1	Very low

Process	*Benefits*	*Disadvantages*
Gas nitriding	Low distortion	Low contact stresses allowed
Ion nitriding	Low distortion, fair torque cap.	Expensive
Carburising & quenching	Highest torque cap.	Practically requires grinding
Carbonitriding	High torque cap.	Relatively medium distortion
Through hardening (Q+T)	Distortions only from WEDM process	Low pitting cap. OR low ductility

To compare various heat treatment processes for the gears, Table 5-3 above was created. Case carburising & quenching of gears produces, in general, the most advantageous mechanical properties, leaving a hard surface (e.g. 60 HRC) with good wear and pitting characteristics, with a softer core of 32 to 48 HRC (Rakhit 2000) for ductility. Through hardening however is more economical, and if WEDM is to be used then it is simpler to through harden the gear blank and WEDM cut to the finished shape, compared to rough cutting using WEDM, carburising & quenching, and finish cutting again with WEDM. The rough cut gear would require angular indexing on the WEDM machine for the finishing pass as it is no longer axisymmetric if the tooth profiles have been rough cut earlier, which might be prohibitively impractical for gears with pitch diameters possibly as low as 15 mm.

Gas nitriding the parts after finish cutting is an alternative as it features low distortion, but as the part grows during the process due to the formation of nitrides in the case (Radzevich 2016), it will still produce a slightly ‘distorted’ part. Gas nitriding is also, due to its shallow case depth, more suitable for wear- and fatigue-resistance rather than for high shock loads or high contact stresses - above approximately 1190 MPa (Rakhit 2000), which may appear in this application. Ion nitriding produces a more ductile case

compared to gas nitriding, which is more suitable for shock loading, and would thus be a viable option, however ion nitriding is relatively expensive. Carbonitriding is a mix between carburising and gas nitriding, featuring slightly more distortion than nitriding, however produces good mechanical properties.

An important variable to account for is the surface produced by the WEDM process. According to a heat treatment partner of the parent organisation (Helintö 2019), the 'secondary hardening' on the surface as caused by the machining process causes the surface metallurgical structure to be 'random/unpredictable' and might make the nitriding process inconsistent throughout the part. Also, if an axisymmetric gear blank is to be e.g. carbonitrided prior to WEDM cutting, the case structure will not follow the contour of the tooth profile and causes the entirety of the teeth to be through-hardened with fairly high hardness values, which again causes brittleness in bending. This effectively means that nitriding or carbonitriding do not seem to be feasible options.

In view of the comparison above, it seems that through hardening of the gears to 'reasonable' hardness values (e.g. 40-50 HRC) will provide the least distortion, while still leaving a strong core depending on the tempering cycle temperature. The failure mode of the gears will invariably be pitting due to the lower surface hardness values chosen, as a trade-off in order to increase ductility. Pitting is a more favourable failure mode compared to bending failure, as pitting does not necessarily cause catastrophic failure and is more easily detectable through visual inspection.

The choice of material will then be Ovako X300 (Table 5-2), balancing elongation with static strength values and hardness. Ovako (2019) suggests an 870 °C austenization temperature for 45 min + oil quench for hardening, followed by a e.g. 400 °C temper for 2 hours to produce a ~51 HRC hardness. The blank may be turned before the austenization process, with an intermediate machining step potentially viable between the heat treatment and WEDM steps, in order to straighten the gear side faces and inner diameters.

5.2 Transmission

As described in Section 5.1.1, a compound planetary gear set will be specified. The planetary carrier would ideally be built into the wheel hub and consist of a single solid piece, performing the functions of the wheel hub and of the planet carrier simultaneously. As well as simplifying the assembly, the load path is then shorter and would not have to travel through connecting members, which would be the case were the planet carrier/wheel hub consist of two pieces. A larger outboard wheel bearing (71815-B-TVH) will be used as described in 5.1.1, and a size smaller wheel bearing (71813-B-TVH) can be used on the inboard side to attempt at compensating out the differences. This can also be beneficial in terms of bearing loads, as the outboard wheel bearing is more heavily loaded in the axial direction when cornering than the inboard bearing[2].

Needle bearings can be used to allow relative rotation between the planets and the planet carrier 'pins' that support the planets. Needle bearings can commonly become starved of oil due to their large aspect ratio, to which Stokes (1992: 156) suggests a method where an oil jet injects oil into the inner bore of e.g. a gearbox shaft, where the oil then centrifuges out through radial holes in the shaft to the inner diameter of the needle bearing. The oil then simultaneously lubricates thrust washers as it exits the needle bearing ends. Thrust washers are commonly used in spur gear gearboxes between faces that feature relative rotation, the washers being made from e.g. stamped steel. A plastic bearing material such as PTFE would be more advantageous than steel for the thrust washers, as it is more forgiving in the absence of lubrication, and as the loads are small. It can also be experimented with using thrust washers that feature radial grooves on one face, to attempt at allowing some circulation of lubricant through the washer when the mating part is pressing against it, in the interest of efficiency. Beernaert (2016) describes a simple channel construction which allows the oil situated inside of the planet carrier to be centrifuged outwards and into the needle bearings.

[2] When cornering, the reaction forces of the outer tyres load the outboard wheel bearings axially, whereas the inner tyres load the inboard wheel bearings axially. Load transfer during cornering then forces the outer tyres to be more heavily loaded, causing the outboard wheel bearings to produce a larger reaction force than the inboard bearings.

The design objectives should be to produce a reliable transmission, which also allows easy disassembly while not compromising aspects such as positive locking. This is especially important in motorsport applications, as maintenance occasionally has to be carried out in fairly primitive conditions, where a unit that is then difficult or ambiguous to assemble has the potential of causing system failure resulting from e.g. human error.

The concept for the transmission unit will be described next.

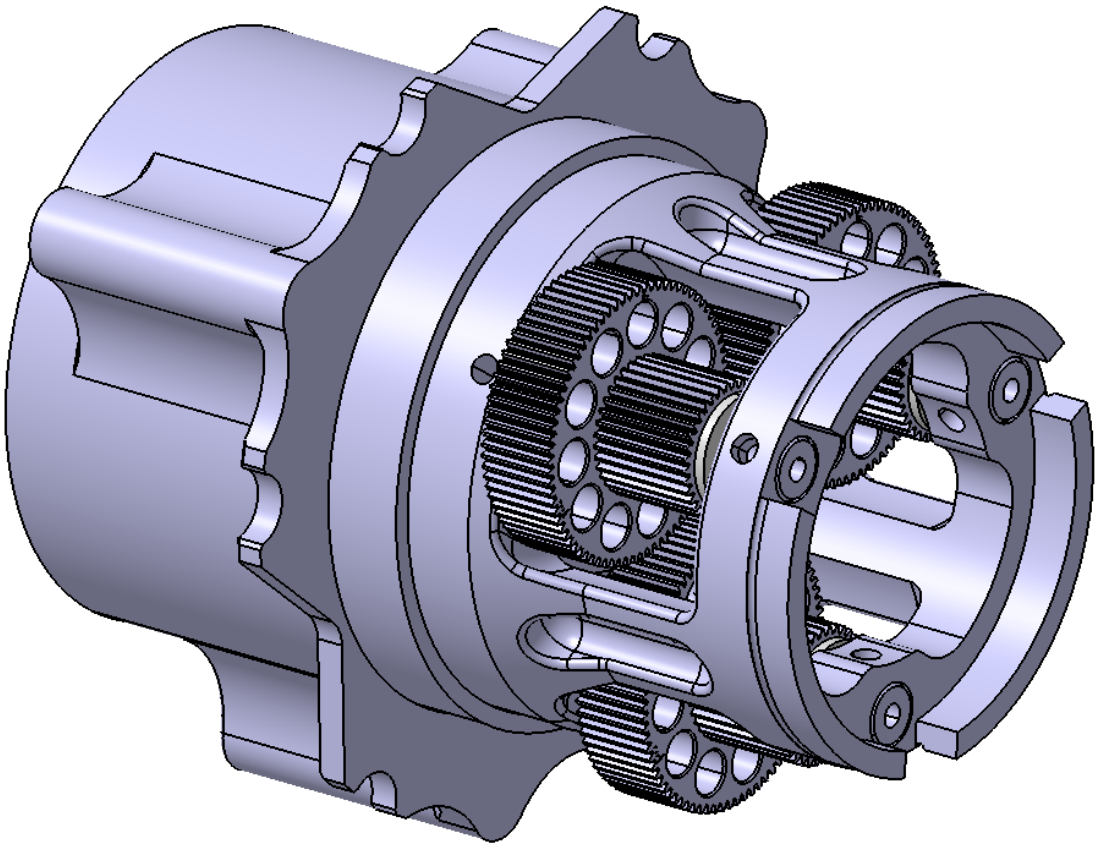

Figure 5-6. Wheel hub/planet carrier

Figure 5-6 displays the combined wheel hub and planet carrier construction. The planet gears are located in radial slots, supported by axial steel planet pins that are lightly pressed into bores in the wheel hub - locking the pins from axial and angular movement. To lock the planet gears together for torque transfer to the smaller planet gears, Beernaert (2016) describes a very simple and elegant method; the external involute tooth geometry of the smaller planet gears are cut out of the larger gears, with the smaller planet gears extending entirely through the larger gears. This then functions identically as a splined connection, providing good torque transfer and centring capability. Since the

WEDM process can cut the splines and the external teeth of the large planet gears in the identical angular positions from part to part, no special considerations for the angular indexing of each pair of planet gears are required. For comparison, if the gears would be pressed together on pure cylindrical surfaces for torque transfer, then two teeth must be specified as ‘registry teeth’ that are then aligned in a jig during pressing in order to ensure angular indexing (Lynwander 1983). The spline connections can be specified with a light press fit to again lock relative axial movement, and the internal teeth of the large planet gears should feature larger diameter addenda and dedenda to clear the top lands and bottom lands of the smaller planet gears, producing flank-centring fits. The planet gear pairs then fit into the axial space provided by the planetary carrier with a small axial clearance, with thrust washers to allow relative rotation of the planet gears with the carrier, as the car corners and forces the planet gears back and forth, contacting either washer at a time.

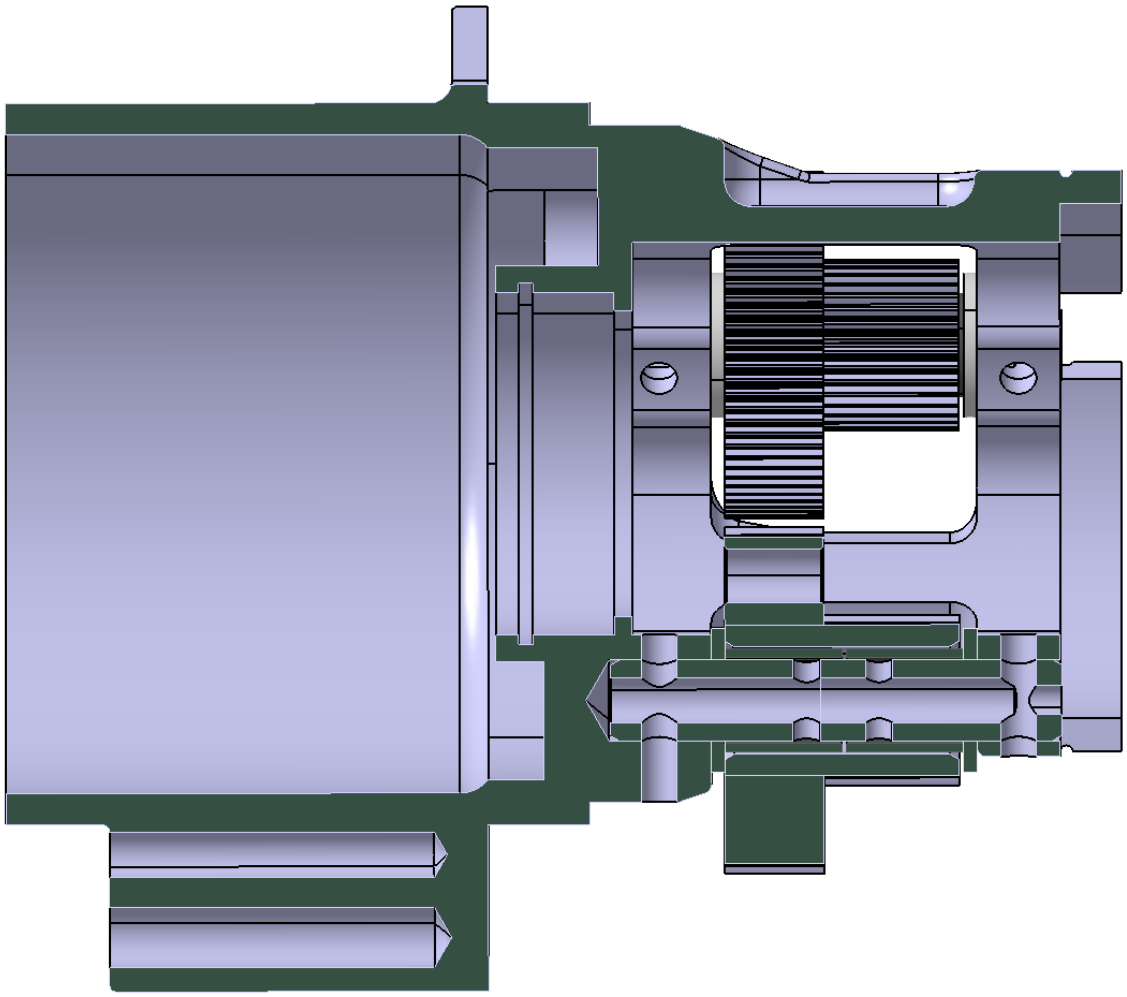

Figure 5-7. Cross-section of wheel hub/planet carrier

Figure 5-7 illustrates more clearly the inner construction of the planet gears. The smaller planet gear is seen extending into the larger planet gear, being supported by two identical needle bearings that are simply inserted next to each other. Situating the needle bearings under the planet gears seems like a simpler solution compared to placing them inside of the bores that are currently intended for the planet pins. The bores would then have to be of larger diameter to fit the bearings (reducing the planet pin diameter can cause manufacturing problems in drilling out the lubrication channel), and steel shells would possibly have to be inserted into the bores to function as wear surfaces, as the wheel hub/planetary carrier would ideally be made of aluminium.

Figure 5-7 also partially displays the lubrication channels for the needle bearings, where the oil travels from the inner diameter of the planetary carrier to the inner diameters of the planet pins and ejecting through the two middle holes of each pin and into the bearings. The radial channels in the wheel hub can be drilled from the outside, with the outer halves of the channels blocked off by the wheel bearings when seated.

As the planet pins are lightly pressed in, one end of the pins can be threaded for extraction, clearing the inner diameter of the pin, e.g. an M4 thread for an Ø5 hole. A tool that fits onto the carrier can then be used to pull the pins out using screws, as shown in Figure 5-8 as an example.

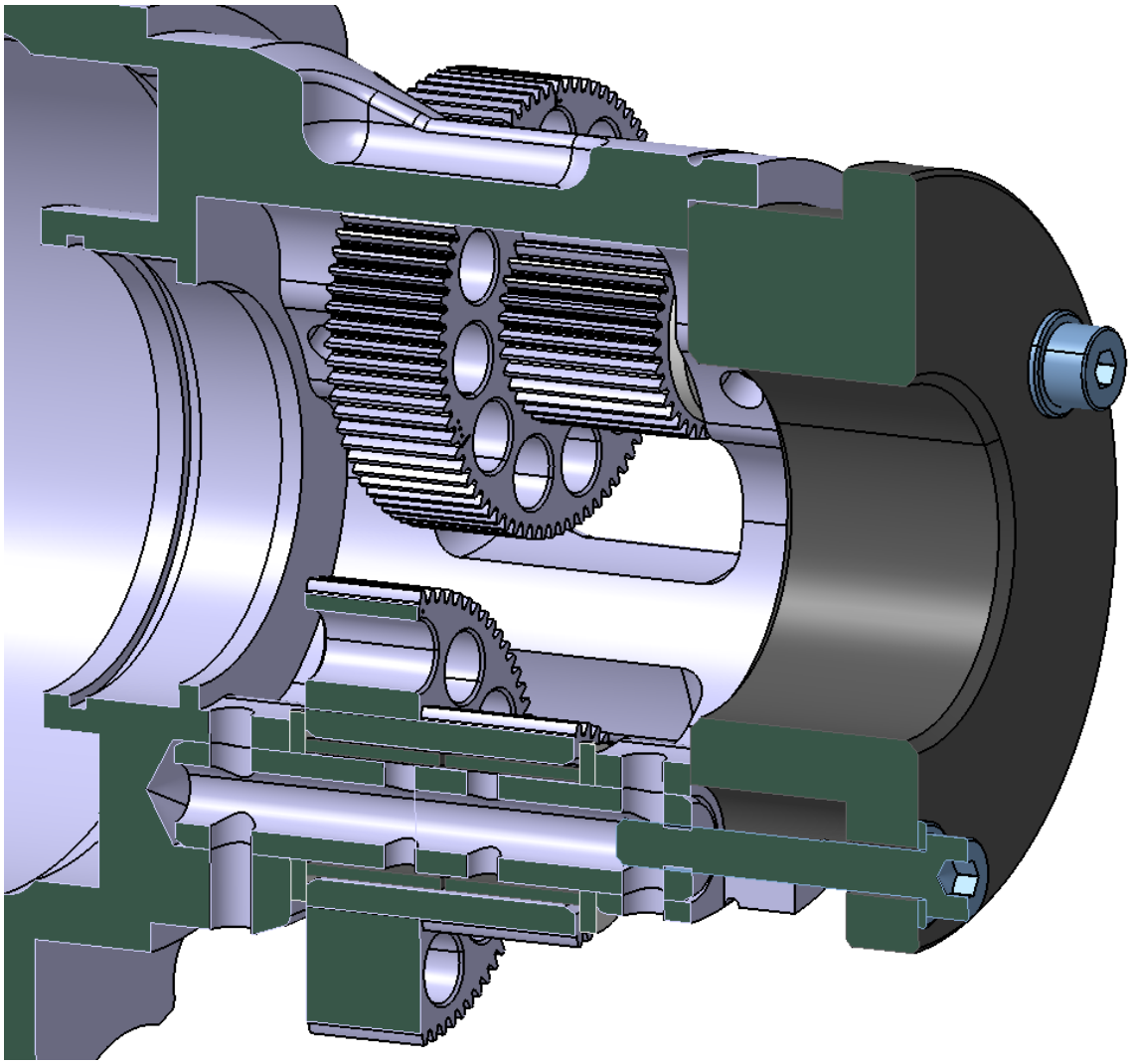

Figure 5-8. Tool to extract planet pins using screws

The wheel hub featuring the bearing construction is shown in Figure 5-9. The two bearings are to be placed in an O-arrangement for moment stiffness. The preloading will employ a similar mechanism which has been used previously for the wheel bearings, consisting of a threaded aluminium nut which is positively locked using a laser cut profile. The laser cut profile locks into the wheel hub on the inner diameter, and features tangs on the outer diameter that fold into at least one slot as provided by the nut. The lock washer can also feature small rubber discs (that are e.g. water cut), that are relatively soft, which can be bonded onto the internal tangs of the lock washer to plug up the remaining open ends of the planet pins, to make the needle bearing lubrication more effective.

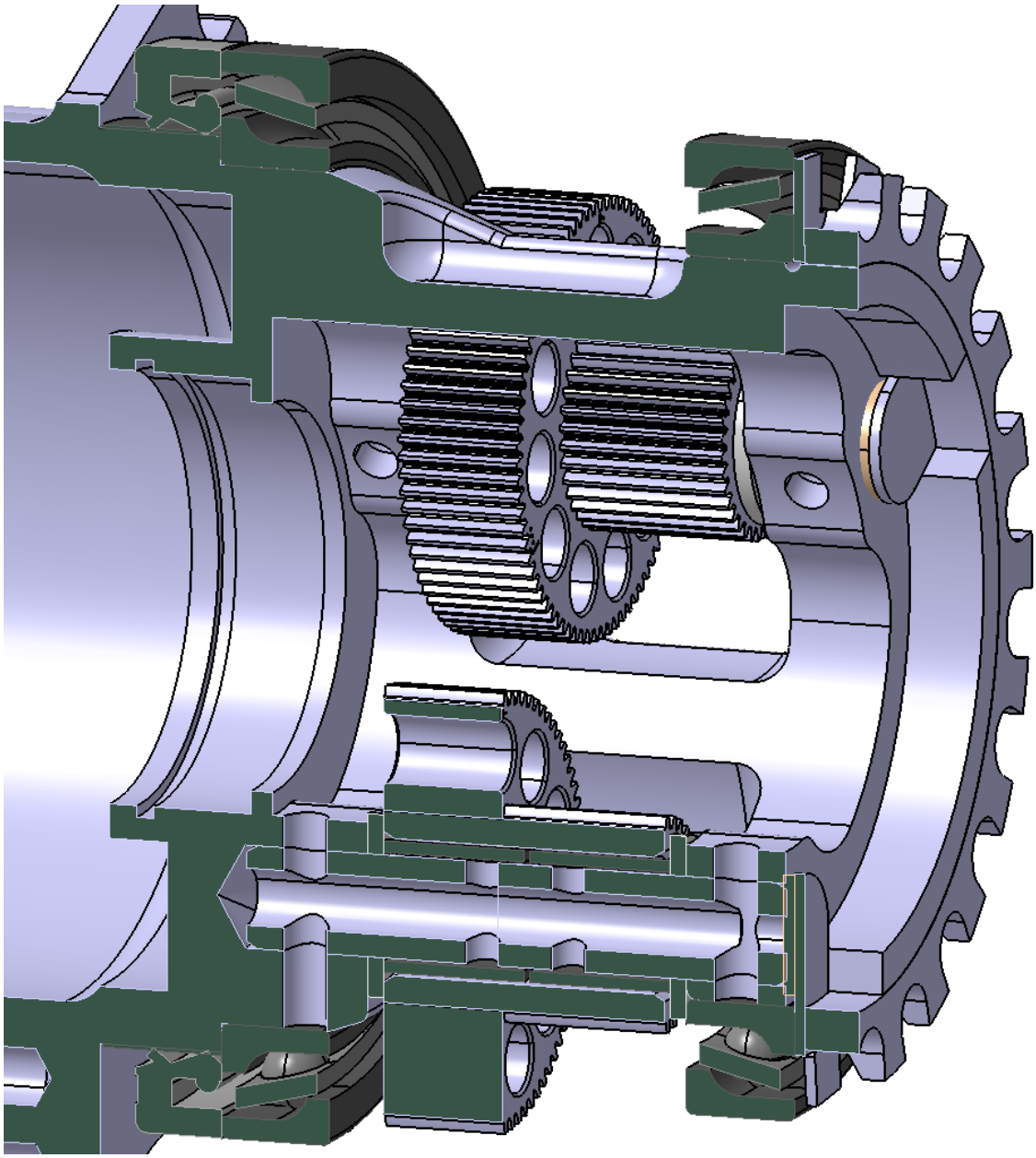

Figure 5-9. Wheel hub assembly with bearing construction shown

The width of the bearing preload nut is significant in this case, as ideally the motor unit will be mounted as close as possible to the inboard wheel bearing. The width of the nut then forces the motor to be located further away, decreasing the compactness of the drivetrain. A preload nut which is threaded on the inner diameter of the planet carrier would be more ideal, with a flange that would reach up to the bearing and preload it, however such a construction would in this case be clumsy as it would be more difficult to positively lock, and it would potentially block the inboard needle bearing lubrication channels. An external preload nut as depicted is then a compromise between compactness and functionality.

The lip seal on the outboard side is chosen to provide a shoulder for the outboard wheel bearing, while fitting in the same housing diameter as the bearing. Spring-less single-lip lip seals have been used in the past for the sealing of transmission oil, with good effect. The absence of a spring could slightly reduce the loss in efficiency that lip seals cause. Aluminium shafts have been used in previous drivetrains for certain lip seal rubbing surfaces, however the surface wears out quickly and creates a groove through which the oil can leak out. The wheel hub could then benefit from using a hardened wear sleeve as offered by many lip seal suppliers, which is pressed onto the lip seal seat of the shaft. The part can also be hard-anodised or electro less nickel-plated for better wear characteristics, although a wear sleeve seems like a simpler solution as the part would then retain its as-machined dimensions.

The ring gear mounting method in the upright is displayed in Figure 5-10. The most important factor for choosing the type of geometrical connection for supporting the reaction torque in the ring gear in this case is machinability. Circular shapes are suitable, as the WEDM process is able to cut the semi-circles as depicted for the ring gear (while also including undercuts for the mating corners), and the fact that matching holes can with ease be drilled & reamed in the upright during the milling process. A light press fit can be specified for the ring gear-upright connection to prevent axial movement. The semi-circle at the top position is Ø6 mm in diameter whereas the rest are Ø5 mm, forcing the ring gear to always be assembled at the particular position depicted.

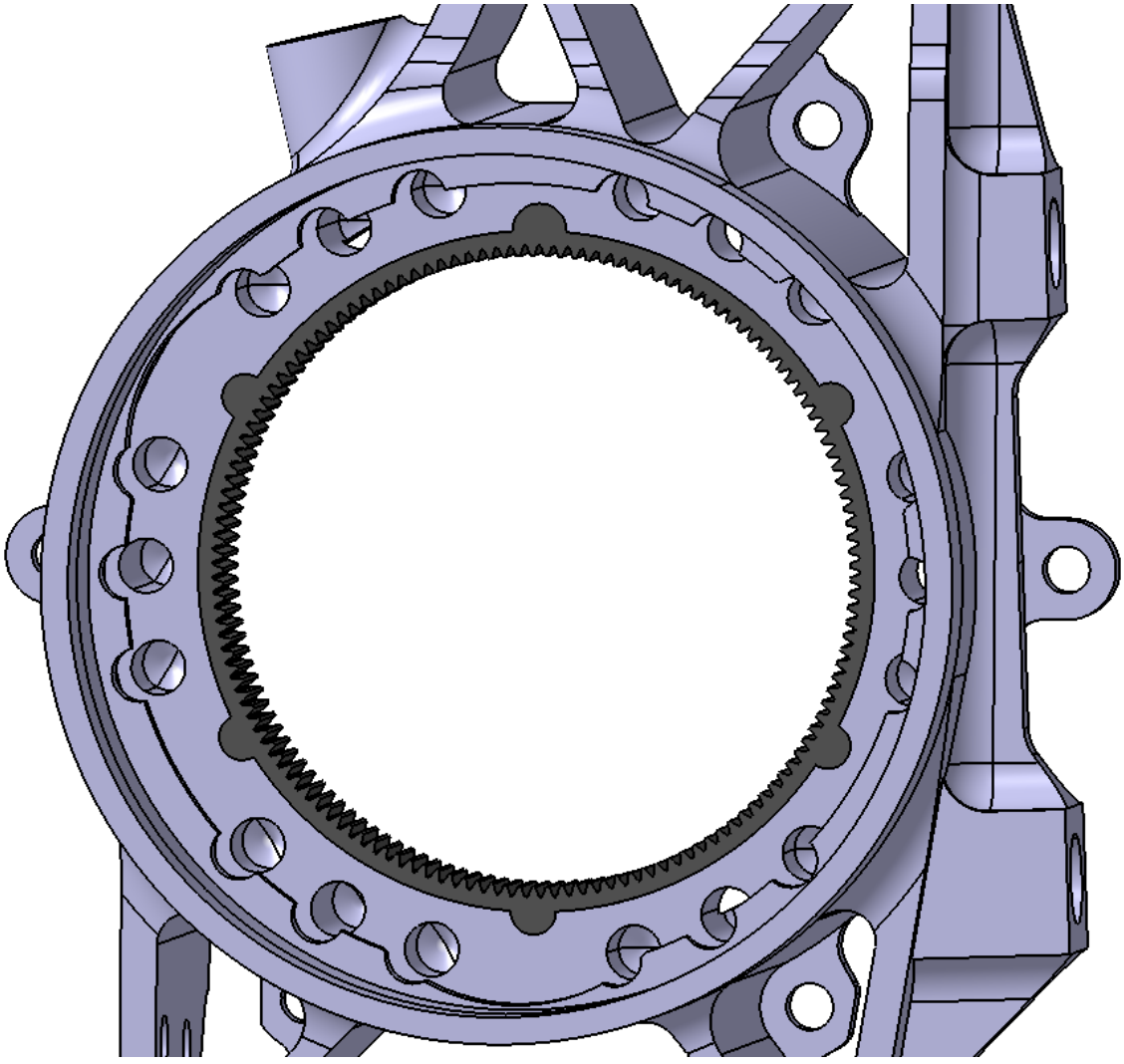

Figure 5-10. Ring gear located in upright

Figure 5-11 displays the transmission as it sits in the upright. A radial O-ring seal that is meant to connect with the motor unit to seal the transmission oil is visible on the right

side. A check cover on the left side of the wheel hub allows for visual inspection of the sun gear-planet gear meshes when attaching the motor unit onto the transmission.

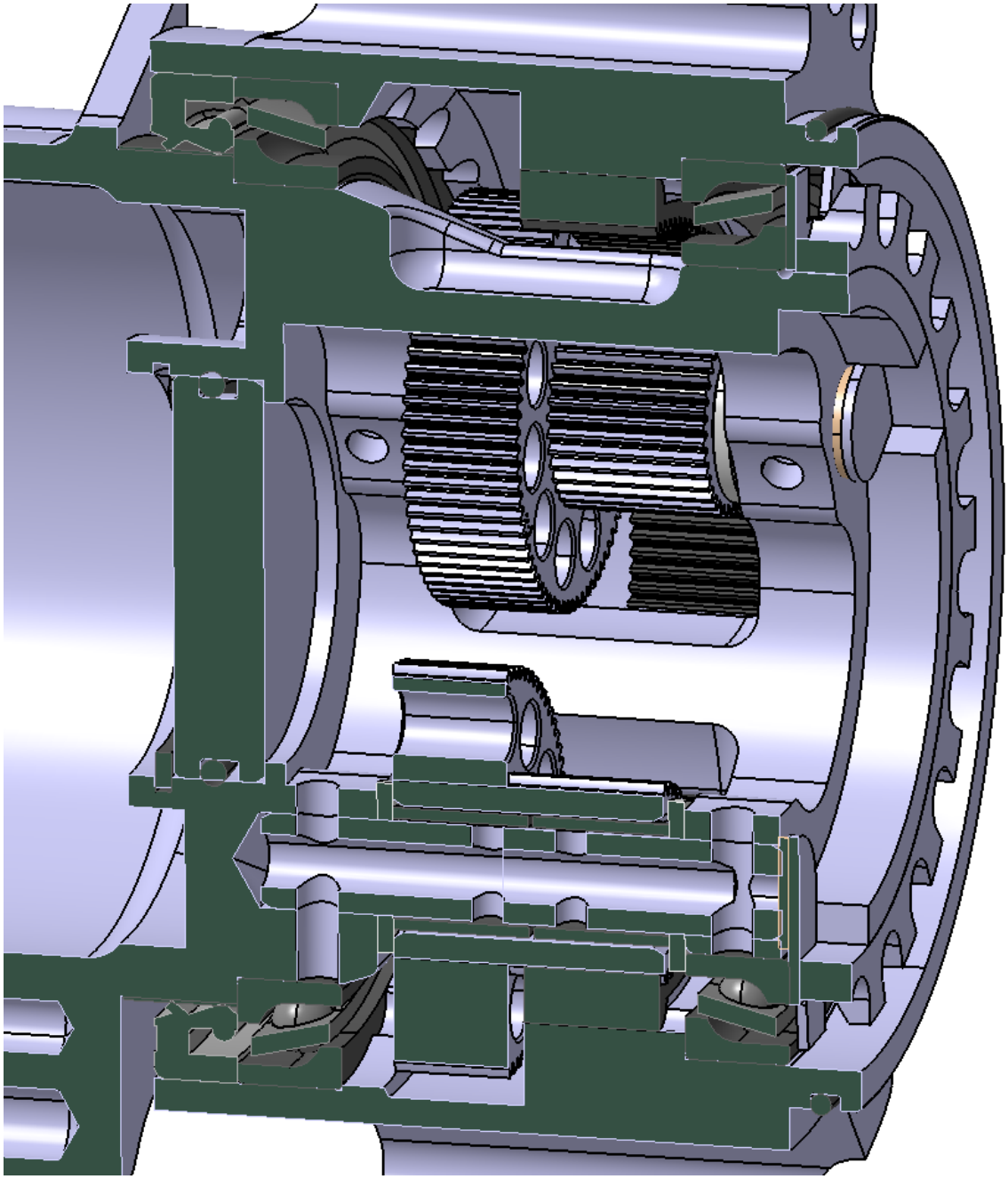

Figure 5-11. Cross-section of transmission assembly in upright

For the assembly and disassembly process, the wheel hub can be assembled separately up until the inboard wheel bearing. The lip seal wear sleeve, the outboard lip seal, and wheel bearing are assembled onto their seats firstly, after which the planets are assembled. Each planet pin could be machined to only feature an interference fit on the area where it mates with the *inboard* wheel hub bore, meaning that the planet pin can be

easily inserted using a clearance fit while assembling the planets, after which the pin is then tapped/lightly pressed into place – while checking that the lubrication channel is indexed in the correct position. This wheel hub unit can then be assembled into the upright. Finally, the inboard wheel bearing can be assembled and preloaded using the preload nut and washer.

Lubrication of the transmission is carried out through splash lubrication using oil. The oil viscosity used in this application might have a larger impact on churning losses, as the carrier rotates and moves the planets through the oil bath, compared to a spur gear transmission where only the teeth continuously displace the oil. Considering the short lifespans of FS transmissions, low specific oil film thicknesses ($\lambda < 1$) may be acceptable, possibly allowing experimentation with low viscosity oils in the interest of reducing churning losses - as viscosity and specific oil film thickness are commonly related to each other (Douglas, Thite 2015). As the oil bath will in this case submerge the lower part of the outboard wheel bearing and lip seal due to their location, a lip seal featuring a spring might be worth testing if the spring-less lip seal described is prone to leaking.

A temperature probe affixed to the upright as shown in Figure 5-12 will sense the oil temperature as the oil is thrown radially outwards. The same hole can also be used for the filling and draining of oil. A magnet situated in the transmission has proven to be useful in the past, as it picks up some of the particles removed from the gears due to normal wear, and has been added here onto the side of the upright.

Currently, an oil breather is not specified as it simplifies the chassis system by then not requiring a rules mandated catch can, which has been employed in past drivetrains. If the lip seals are prone to leaking due to pressure differences between the air in the transmission and ambient/rotor environment air, then the temperature probe can be replaced with a breather.

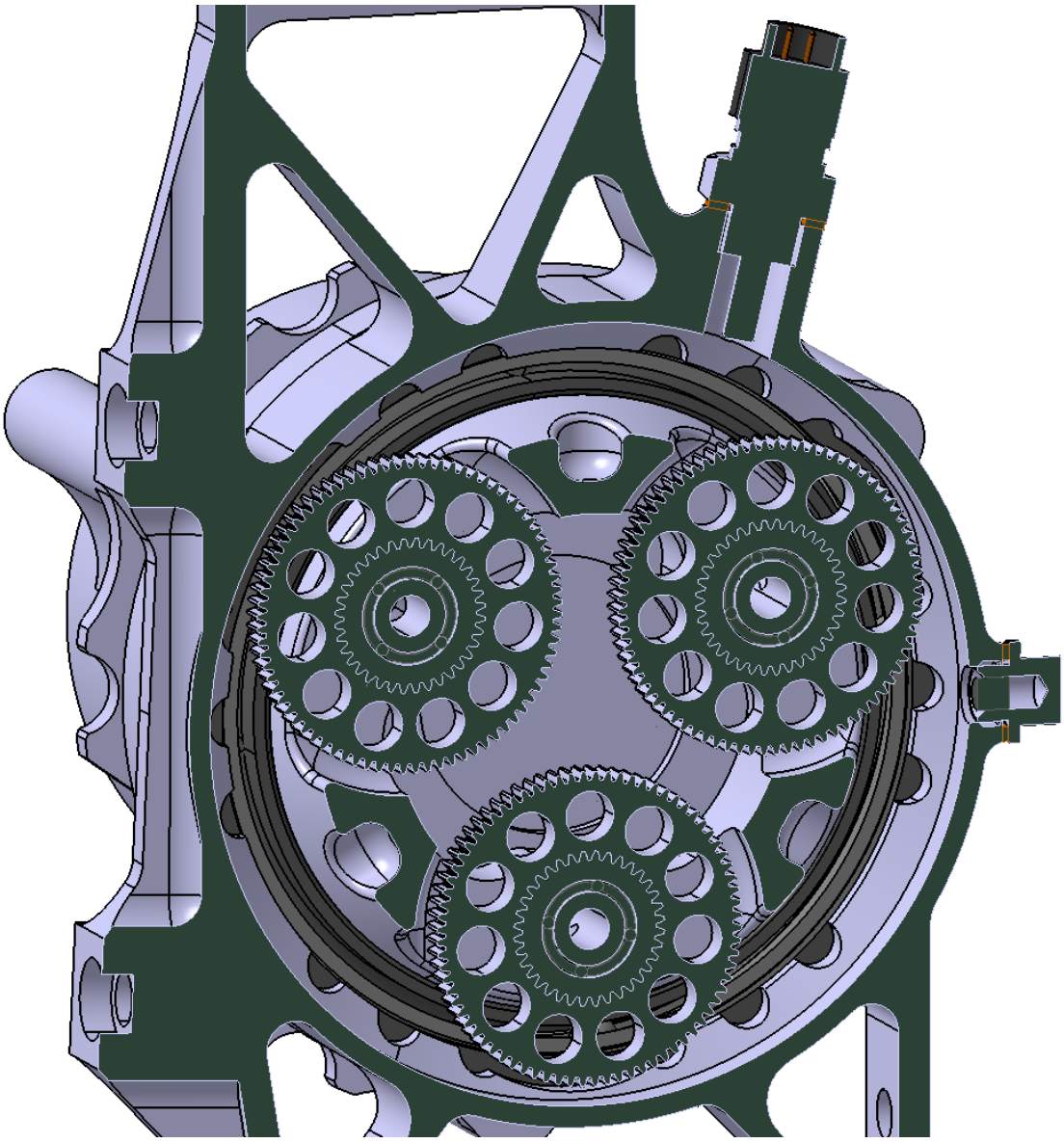

Figure 5-12. Axial cross-section of transmission

The assembly and timing of the gear train is depicted in Figure 5-13. Timing marks are used for the large planet gears and sun gear with dots showing the numbers 1, 2 and 3. The large planet gears are able to be manufactured identically without requiring each one to feature unique markings, simplifying manufacturing. When the planet carrier is assembled with the planet gears into the ring gear (upright), the large planet gears are rotated about their planet pins until the timing marks line up. A sun gear with corresponding timing marks can be used to align the planet gears and keep them in that position during insertion into the ring gear. Although the number of teeth of the gear train allow the planet pairs to be timed and manufactured identically to each other, aligning the gears during assembly in this fashion ensures that no ‘false’ meshes are found. False

meshing can occur as the gears can be physically forced into mesh if sufficient backlash is present in the system, which causes the gears to tend to bind at some point when rotating (Lynwander 1983).

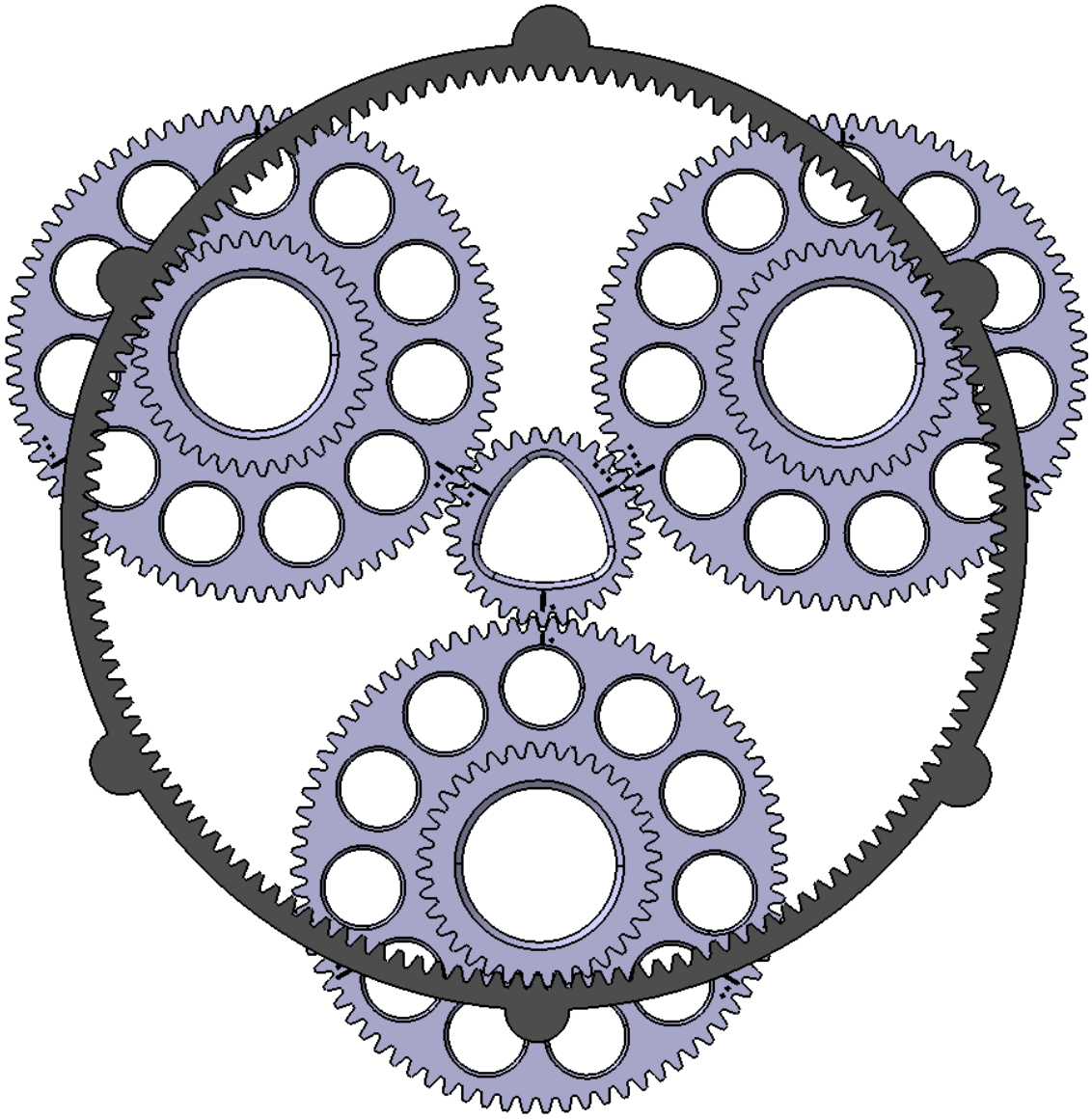

Figure 5-13. Assembly and timing of gear train

5.3 Motor unit

As mentioned in Section 4.1, motors only featuring a stator and rotor will be supplied, and bespoke casings and shafts need to be designed. The 1FE1041-6WM motors that will be used feature a maximum operational speed of approximately 16 000 rpm, and the bearing and seal selection has to especially account for this higher rotational speed. The shaft critical speeds must also be determined during the detail design -phase, with the

motor shaft ideally not passing through any critical speeds at any time during operation. As shaft critical speeds vary with bearing load, the critical speeds have to be determined when the bearings are lightly loaded.

In previous drivetrains, Heidenhain absolute rotary encoders have been used that have worked well, as they are compatible with Siemens motor control units. For the higher speeds of the specified motor, optical absolute rotary encoders like the ones previously used are usually not capable of higher speeds, and many models feature maximum speeds of 12 000 - 15 000 rpm (Heidenhain 2015). Incremental magnetic encoders feature more flexibility in this regard and are fairly robust, however the incremental characteristics of the encoder and compatibility with Siemens control units may cause complications. RLS provides incremental encoders that seem suitable, with high environmental protection ratings and robust constructions, and an RLS RM44 (RLS 2019) incremental magnetic encoder will be specified for the motor unit.

Deep groove ball bearings can simply be used for the motor shaft bearings, as the motors do not theoretically produce any axial loading. The motor shaft bearings have in the past been preloaded - to a fairly low force - to increase the stiffness and life of the bearings. The preloading has been carried out through the use of rubber washers that press on the outer race of the non-locating bearing situated on the Non-Driven End (NDE) of the motor, displacing the outer race and preloading the locating bearing on the Driven End (DE) of the motor as well. Because of the relatively high stiffness values seen in typical industrial rubber materials, manufacturing tolerance stack-up of the shaft and all casings has the effect of heavily increasing or decreasing the resulting bearing preload. Metallic preload springs with lower spring constants than solid rubber washers are then preferred, producing a more constant preload.

The DE bearing can be non-sealed and use the same oil as the transmission, with a rotary lip seal behind it to seal the rotor environment from the transmission oil. For load-sharing purposes of each sun gear-planet gear mesh, the DE bearing is ideally specified with a larger radial internal clearance than what is normally supplied, giving a more compliant sun gear[3]. The NDE bearing needs to be lubricated for life, and sealed with e.g. a

[3] Deep groove ball bearings are normally supplied with a ’CN’ designation, however ideally a ‘C4’ designation is specified. The radial clearance values for the two designations for a d20 bearing is 5-20 µm for CN, and 20-36 µm for C4 (Schaeffler 2019)

double non-contact gap seal (-2Z suffix), which are more suitable for high speeds compared to double lip sealed bearings (-2RSR suffix). The rotor environment is fairly free from contamination, allowing the use of non-contact seals. The NDE bearing should be of smaller diameter as grease-lubricated bearings are commonly limited to smaller tangential speeds compared to open-ended, oil-lubricated bearings.

The connections for the water-cooling system for the motors have currently been sealed using zip ties or sealed automatically using barbed push-in connections. The cooling system for the current drivetrain is disassembled rarely, and zip ties have proven to work fairly well once the system has been inspected for leaks. An outboard motor might require disassembly more often due to its location, placing a higher demand on incorporating proper leak-tight connectors for the water circuit.

Figure 5-14 displays the motor unit as a whole. The DE bearing shield is seen on the left side with the motor shaft and sun gear protruding out. The DE bearing shield is attached onto the water cooling jacket sandwiched in the middle.

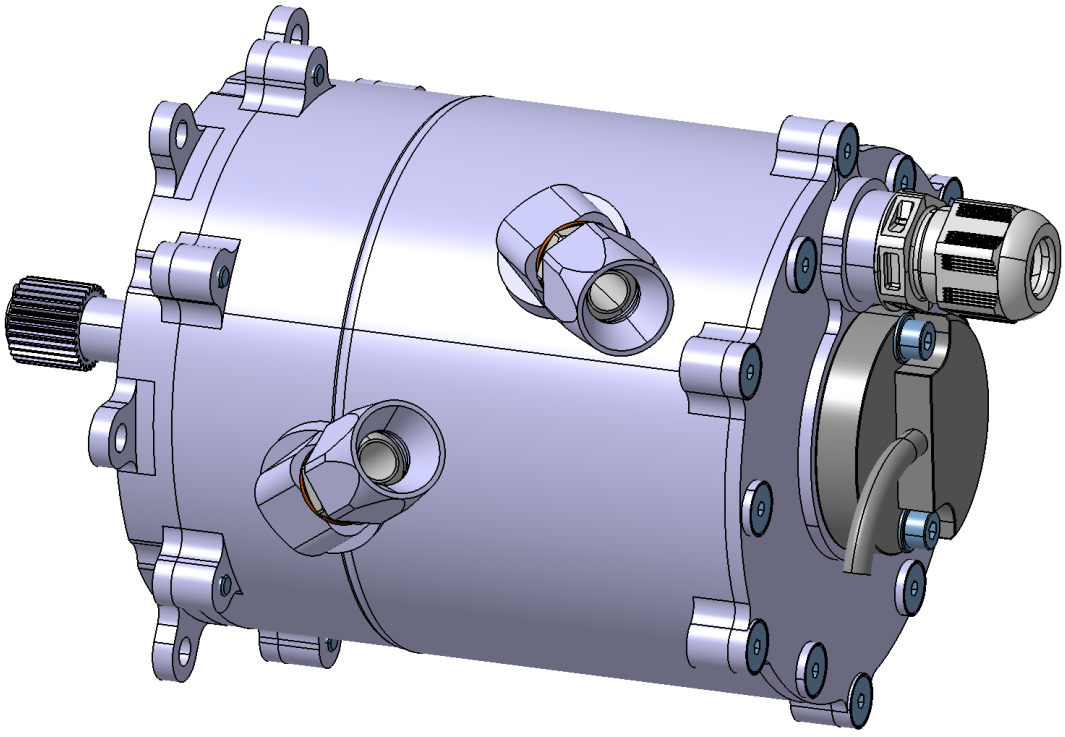

Figure 5-14. Motor unit

The non-driven-end bearing shield on the right side features the RM44 encoder on the shaft centreline, and above it, an industry-standard plastic cable gland is threaded onto the bearing shield to provide a sealed outlet for the motor cables and temperature sensor wires. The stator as supplied *only* features threaded holes for motor casing attachment on one end, in this case the NDE. The DE bearing shield is then attached to the water cooling jacket, which is attached to the NDE bearing shield, which in turn is attached onto the stator. This is not ideal, however definitely simpler in terms of packaging compared to rotating the stator around 180° and attempting to provide a sealed route for the motor cables, which would then be pointing at the transmission. The unused attachment points on the DE bearing shield in Figure 5-14 is intended for attaching the motor unit onto the upright. When the motor unit is assembled onto the upright, the sun gear is firstly placed into mesh with the planets, after which the unit is inserted fully and fastened.

The water cooling inlet/outlet connections as depicted in Figure 5-14 are intended to provide for a more reliable water hose connection method. The connection method uses industry-standard AN connectors for the hoses, where the outermost nut, as depicted with a hexagonal shape, is threaded with the hose onto the rest of the assembly which is attached to the cooling jacket.

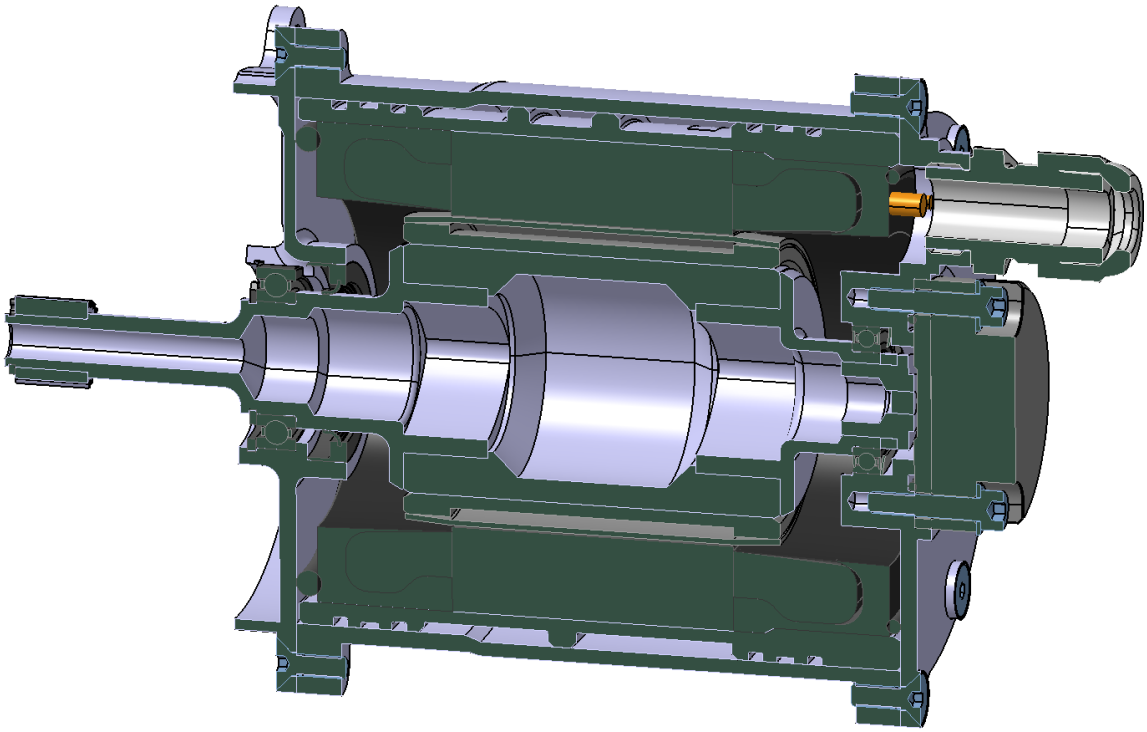

Figure 5-15. Cross-section of motor unit

Figure 5-15 displays a cross-section of the motor unit. The rotor as supplied is visible right inside of the stator, which is heat shrunk onto a bespoke ferritic rotor sleeve, required to be of 4 mm wall thickness as per the suppliers instructions. The rotor sleeve connects with two shafts, a DE shaft and a NDE shaft, through P3G polygons for torque transfer and a light press fit to restrain axial movement. The complete motor shaft is then made up of 3 pieces with the rotor shrunk onto it, which allows the shaft to feature a hollow inner geometry for lightness and to increase the critical speeds of the shaft. The bearing seats and lip seal surface of the motor shaft has to be finish machined when the shaft ends are pressed in to reduce run-out. The motor shaft with the rotor assembled then has to be balanced to an ISO 1940: G2.5 rating (Siemens 2016), where the axial faces on the motor shaft ends that mate with the rotor sleeve provide surfaces that can be cut or ground into for balancing.

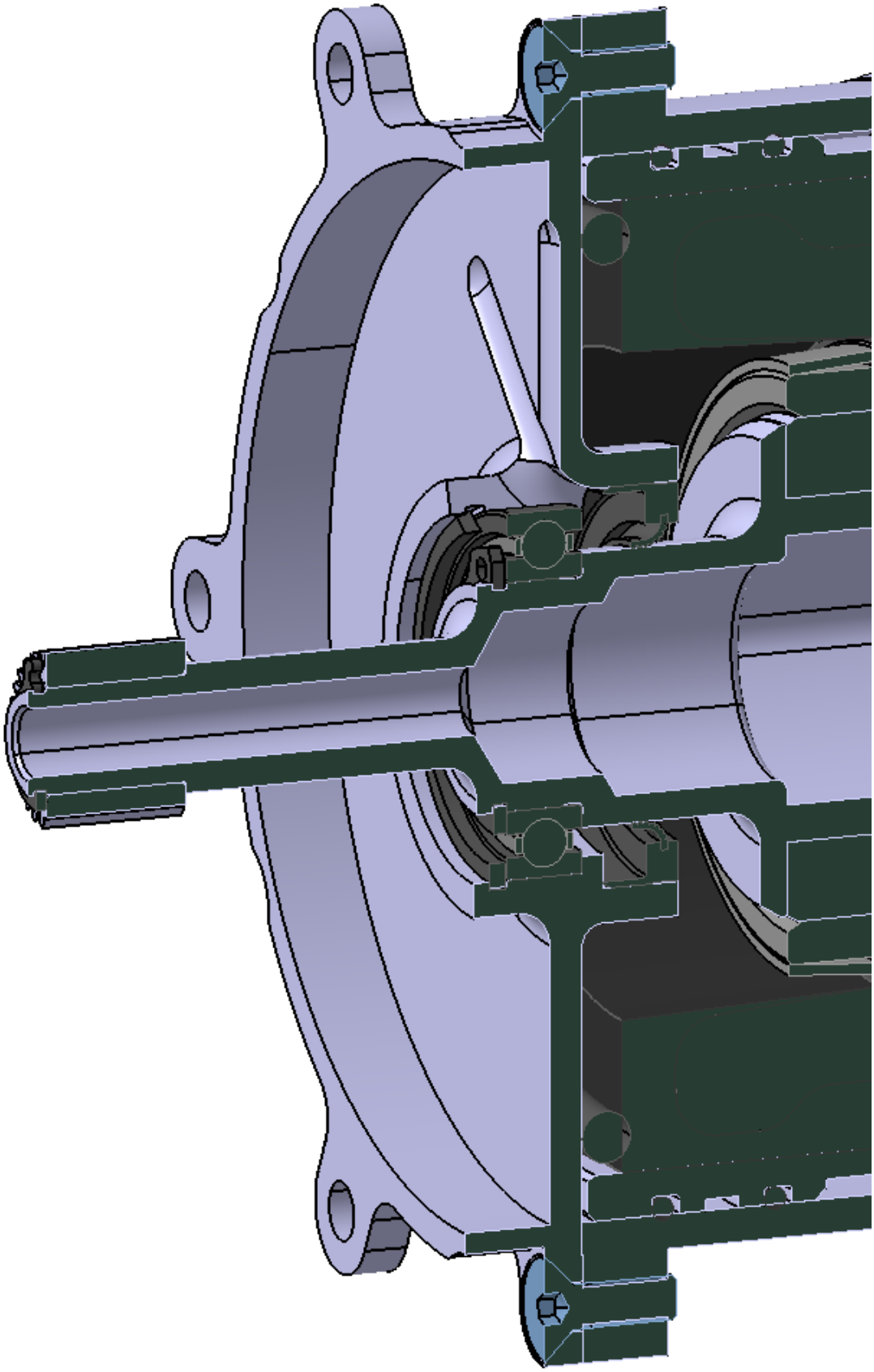

Figure 5-16. Cross-section of DE of motor unit

Figure 5-16 displays the DE side of the motor unit. The sun gear is connected using a P3G connection and secured using a circlip. The locating bearing shown is locked similarly using circlips. The rotating circlip easily manages the rotational speeds of the shaft, however a rotary lip seal capable of 20 m/s tangential speeds is required, to which a Turcon Varilip PDR –lip seal is specified (Trelleborg 2019), capable of 60 m/s tangential speed. A radial cut-out is provided at the top of the bearing shield to attempt at creating an oil-circulation effect, where the oil drains into the cavity behind the bearing as it flows down the walls, and is then pumped back into the front of the bearing to the oil bath. The shallow radial grooves extending further up the bearing shield are intended to collect some of the oil flowing down the walls and attempt at guiding it to the main oil channel. As the channel has to be assembled in the upright position, the mounting holes on the DE bearing shield for the motor unit to mount onto the upright are placed at slightly varying angular intervals to enforce unambiguous assembly. The bearing shield seals the rotor environment using an axial O-ring mating with the stator, along with two O-rings per side on the stator sealing the cooling jacket from water egress.

Figure 5-17 displays a close-up of the NDE construction. The encoder is attached to the NDE bearing shield and seals the rotor environment with an axial O-ring. A small magnet attached onto a separate aluminium insert on the motor shaft end drives the encoder for position sensing. The separate encoder magnet insert is required to be non-magnetic according to manufacturer specifications (RLS 2015). To compensate for manufacturing tolerances, the distance of the axial face on the NDE bearing shield mating with the encoder, to the magnet can be measured on each individual motor unit. Bespoke aluminium shims can then be turned and assembled onto each aluminium insert, in order for the magnets to be more precisely at the desired offset to their encoder faces, as the nominal offset between the two components is only 0.5 mm.
Visible in Figure 5-17 is also the NDE bearing and its preload spring, displacing the outer ring.

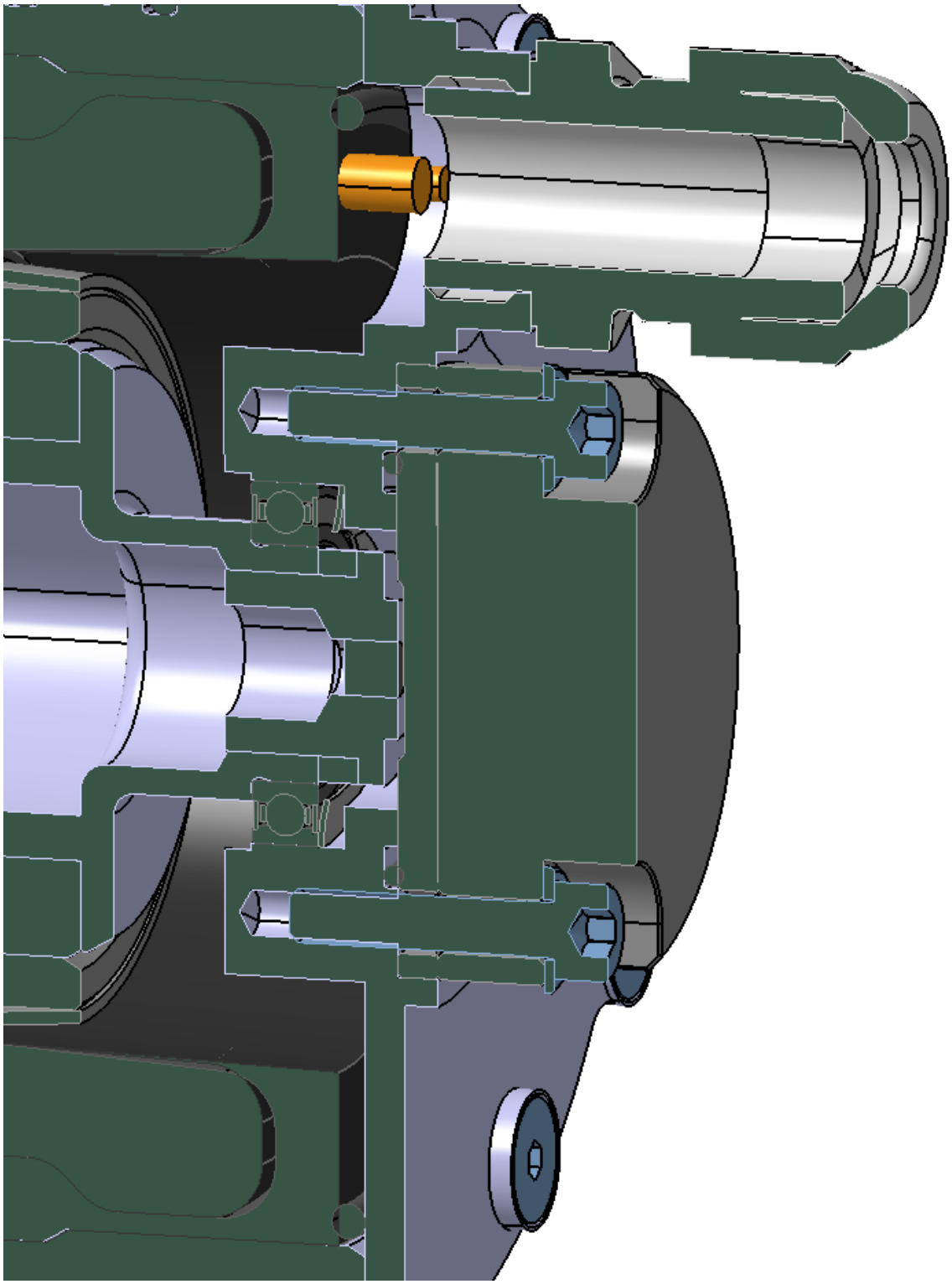

Figure 5-17. Cross-section of NDE of motor unit

5.4 Drivetrain assembly

The complete drivetrain is shown in Figure 5-18. The motor unit can be bolted onto the upright and positively fastened using nylock nuts/k-nuts as shown.

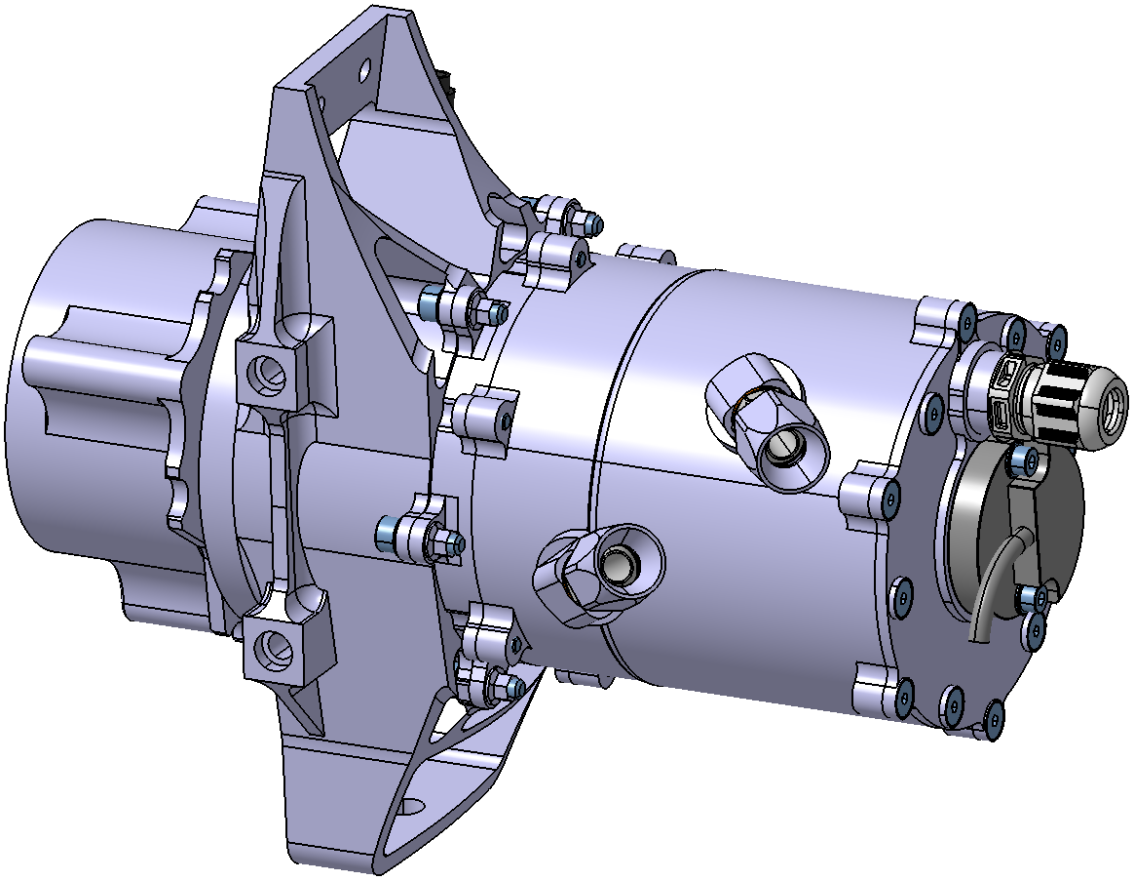

Figure 5-18. Complete drivetrain

Table 5-4 displays a mass overview of the concept system, based on the CAD models. The stressing programme will invariably change the mass of components, however it is still a fair indication of mass. As the transmission unit includes the modified upright and wheel hub while the value for 'HPF019 drivetrain' does not, the mass of the transmission is 'exaggerated'. If only the *change* in the mass of the upright and wheel hub is accounted for in the transmission mass and not the entire components, then the value reduces to 0.9 kg, decreasing the overall drivetrain mass to 19.5 kg (Appendix 2).

Comparing the change in the total mass of the car is of small value and difficult to predict, as switching to four outboard wheel motors causes large changes to the overall design of other sub systems, increasing e.g. the amount of inverters needed (although rated for less power), and requires the water cooling tubing to be extended, increasing mass,

while at the same time the mass of the frame is reduced as the rear drivetrain compartment is non-existent.

Table 5-4. Overview of system mass

System mass	*Mass (kg)*
Transmission unit	1,7
Motor unit	4,0
Drivetrain assembly	5,7
Drivetrain assembly x4	22,7
HPF019 drivetrain	47,5
Difference	52 %

Figure 5-19 shows a cross section of the drivetrain. The overall concept is of a fairly simple and compact design, and seems to feature relatively low mass. Mass can be reduced further through developing and optimising e.g. stressed components, and mass reductions are more beneficial in this case as most components gets multiplied by 4 instances in the car. The largest compromises made relate to the reduction ratio of the gear set as it deviates by 9.9% from the desired ratio. The motor shaft construction is from a design and manufacturing point of view less ideal, as it requires a geometrical connection for each shaft end, increasing mass, and requiring more manufacturing operations than a one-piece construction. The final mass saving is however significant, offsetting the negatives. The encoder construction is more robust and lighter than the optical encoder currently used, and fits into the stator well. Focus has been placed on the lubrication of the bearings to attempt at increasing bearing efficiency. Assembly conditions have been considered fairly extensively, and a range of tools have been modelled to attempt at making the assembly and disassembly processes more successful.

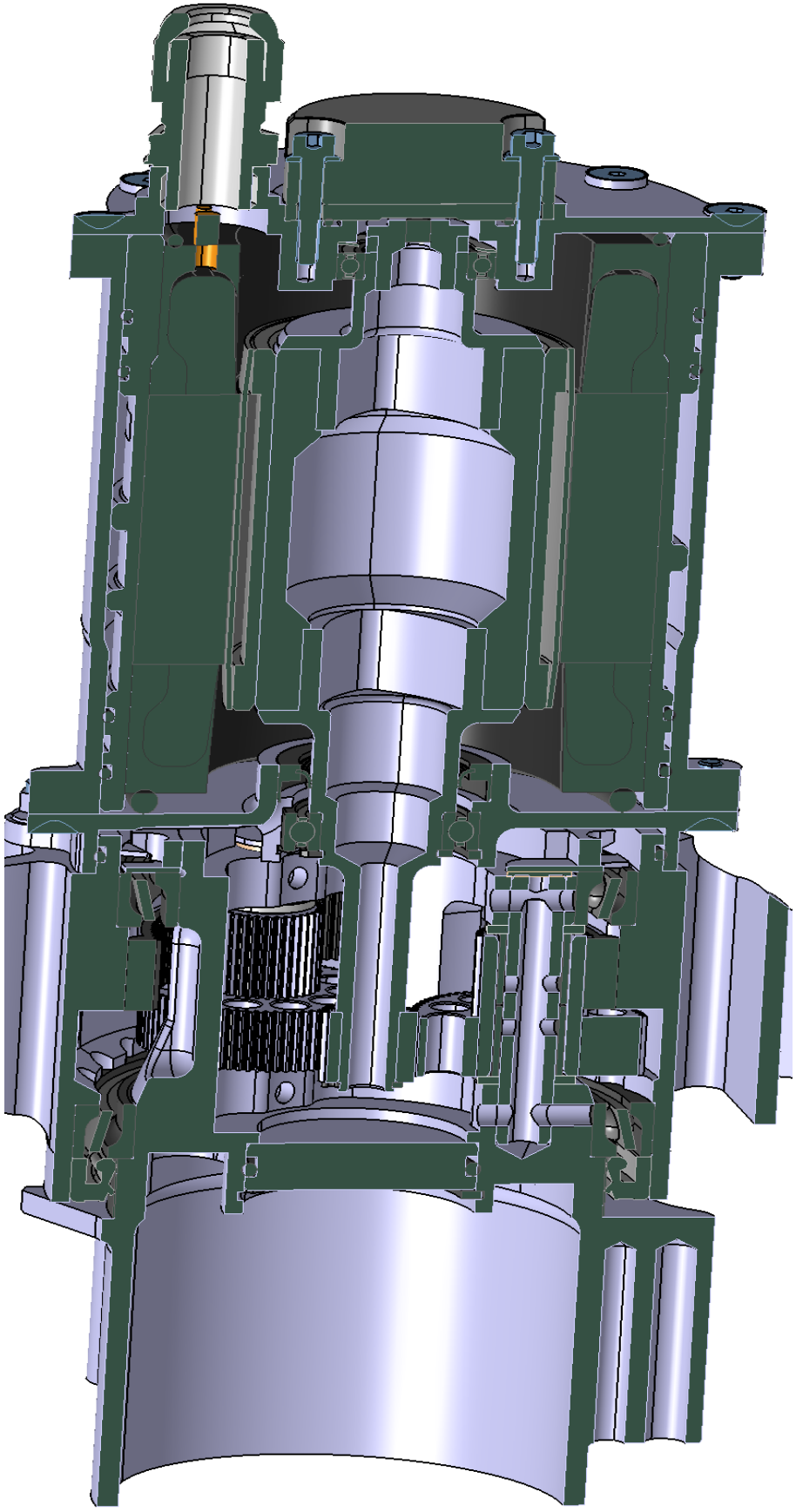

Figure 5-19. Cross-section of drivetrain

Although the crude lap time model already indicates an increase in the performance of the car compared to the current HPF019 car, the author believes that performance can be increased further by making full use of other benefits that four individually driven motors offers. Some of these benefits can be listed as four wheel regenerative braking, to increase the available power in the Endurance event, and torque vectoring, mainly to increase the yaw rate of the car. Torque vectoring can be initially implemented as a function of steering wheel angle, in order to get a crude model working to trigger further development.

6 Conclusions and recommendations

As a result of the work described above, a simple and compact drivetrain concept was produced, which attempts at balancing these aspects as well as manufacturability, assembly conditions, efficiency, and robustness.

The motor architecture and desired transmission reduction ratio have been chosen based on simulation results and the packaging of the components. A load case has been developed based on the data gathered from previous operation, which can be used in the stressing programme to represent real-life conditions more precisely. The type of transmission was chosen to be a compound planetary transmission, suitable for the gear ratios and packaging conditions desired. The number of teeth of the gear set satisfies various geometrical conditions, and the manufacturing method, material, and heat treatment chosen for the gears offer a compromise between the costs, strength, ductility, and accuracy.

To develop the system into a detailed design, which can then be manufactured and tested, the next step is to move into the component-level design phase and to refine and optimise the individual components for e.g. durability. The stressing of the gears and the more critical components should feature a fairly high safety factor, e.g. 2, since a drivetrain component failure is catastrophic and will render the spare parts useless if they too are under-dimensioned. The motor shaft dimensions should also be considered for critical speed, ideally placing the first critical speed beyond the operational maximum of the system.

In conclusion, the design suggested requires that care be taken when assigning tolerances to each dimension of each component, as thoughtful tolerances and fits will ensure that the final real-life assembly resembles the original design intent as precisely as possible. Tolerances and fits chosen through indifference, however, may have the potential of creating a system that looks good as a CAD model, but has to be compromised too heavily during the assembly phase to function well.

7 List of references

Aune, P. A. (2016) *a Four Wheel Drive System for a Formula Style Electric Racecar* [online] available from: <https://brage.bibsys.no/xmlui/bitstream/id/416418/14193_FULLTEXT.pdf> [20 April 2019]

Beernaert, T. F. (2016) *Gear Transmission Design and In-wheel Packaging for a Formula Student Race Car* [online] available from: <https://www.researchgate.net/publication/326575526_Gear_transmission_design_and_in-wheel_packaging_for_a_Formula_Student_race_car> [20 April 2019]

Danielsson, O., Jonsson, I., Hansson, E., Mannerhagen, F., Molander, P., Olofsson, N., Pettersson, J., Pluto, A., Sahlin, G. (2013) *Design of Electrical Powertrain for Chalmers Formula Student with Focus on 4WD versus RWD and Regenerative Braking* [online] available from: <http://publications.lib.chalmers.se/records/fulltext/191837/191837.pdf> [20 April 2019]

Douglas, C. E., Thite, A. (2015) '*Effect of Lubricant Temperature and Type on Spur Gear Efficiency in Racing Engine Gearbox across Full Engine Load and Speed Range'. Journal of Engineering Tribology 0(0) 1-19*

Dowling, N. E. (2013) *Mechanical Behavior of Materials.* 4th edn. Essex: Pearson Education Limited.

Formula Student Germany. (2018) *Results FSG 2018* [online] available from: <https://www.formulastudent.de/fsg/results/2018/> [08 April 2019]

Formula Student Germany. (2019) *Formula Student Rules, Version 1.1, Rev-713* [online] available from: <https://www.formulastudent.de/fileadmin/user_upload/all/2019/rules/FS-Rules_2019_V1.1.pdf> [24 June 2019]

Heidenhain. (2018) *Rotary Encoders* [online] available from: <https://www.heidenhain.com/fileadmin/pdb/media/img/349529-2I_Rotary_Encoders_en_01.pdf> [24 June 2019]

Helintö, M. (2019) *Heat treatment of miniature gears* [email] to Asplund, A. [16 May 2019]

Hynninen, A. (2017) *Planeettavaihteiston Suunnittelu Formula Student -Kilpa-autoon [The Design of a Planetary Transmission for a Formula Student -Race car]*. Helsinki: Metropolia University of Applied Sciences

Kish, J. (1997) *Kish Method for Determination of Hunting Mesh* [online] available from: <https://www.geartechnology.com/issues/0597x/kish.pdf> [06 June 2019]

Kucinski, W., Liang, R., Davis, C., Masucci, M. (2017) *ME 351 – Formula Electric In-Hub Motor System for Formula SAE Electric* [online] available from: <https://static1.squarespace.com/static/57e8888fc534a547699d733d/t/5966f641579fb37769b4c6b3/1499919950515/WR-217e+In-Hub+Motor+System.pdf> [20 April 2019]

Lankila, T. (2017) *Formula Student Electric -Kilpa-auton Voimansiirron Suunnittelu [The Design of a Drivetrain Unit for a Formula Student Electric -Race car]*. Helsinki: Metropolia University of Applied Sciences

Lynwander, P. (1983) *Gear Drive Systems – Design and Application*. New York: Marcel Dekker, Inc.

Müller, H. (1982) *Epicyclic Drive Trains*. Detroit: Wayne State University Press

Ovako. (2014) *Ovako IQ-steel X300* [online] available from: <https://www.ovako.com/PageFiles/134/IQ-Steel%20X300.pdf> [17 May 2019]

Radzevich, S. P. (2016) *Dudley's Handbook of Practical Gear Design and Manufacture.* 3rd edn. Boca Raton: CRC Press

Rakhit, A.K. (2000) *Heat Treatment of Gears*. Ohio: ASM International

Rao, R. S., Mathew, K. A., Rao, G. S. (2015) *Optimization of Wire EDM Parameters to Achieve a Fine Surface Finish.* International Journal of Research and Innovation. 118-124

RLS. (2019) *RM44/RM58 - Up To 13 Bit Encoder Base Unit* [online] available from: <https://www.rls.si/en/rm44-up-to-13-bit-encoder-base-unit> [5 June 2019]

RLS. (2015) *RM44 Magnetic Encoder Base Unit* [online] available from: <https://www.rls.si/fileuploader/download/download/?d=0&file=custom%2Fupload%2FData-sheet-RM44-encoder.pdf> [13 June 2019]

Schaeffler. (2019) *Deep Groove Ball Bearings* [online] available from: <https://medias.schaeffler.com/medias/en!hp.info/618> [14 June 2019]

Siemens. (2016) *Hardware Installation Manual – Simotics Synchronous Built-In Motors M-1FE1* [online] available from: <https://support.industry.siemens.com/cs/attachments/109745110/1FE1_hw_inst_man_1216_en-US.pdf?download=true> [13 June 2019]

Simionescu, P. A. (1998) *A Unified Approach to The Assembly Condition of Epicyclic Gears.* Transactions of the ASME, Vol. 120, September 1998. 448-452

Stokes, A. (1992) *Manual Gearbox Design*. Oxford: Butterworth-Heinemann Ltd

Trelleborg. (2019) *Turcon Varilip PDR* [online] available from: <https://www.tss.trelleborg.com/en/products-and-solutions/rotary-seals-or-shaft-seals/turcon-varilip-pdr> [11 June 2019]

Uddeholm. (2007) *EDM of Tool Steel*. 3rd edn.

8 Appendices

Appendix 1 – Vehicle speed vs. elapsed time, OptimumLap simulation, Autocross Spain 2018

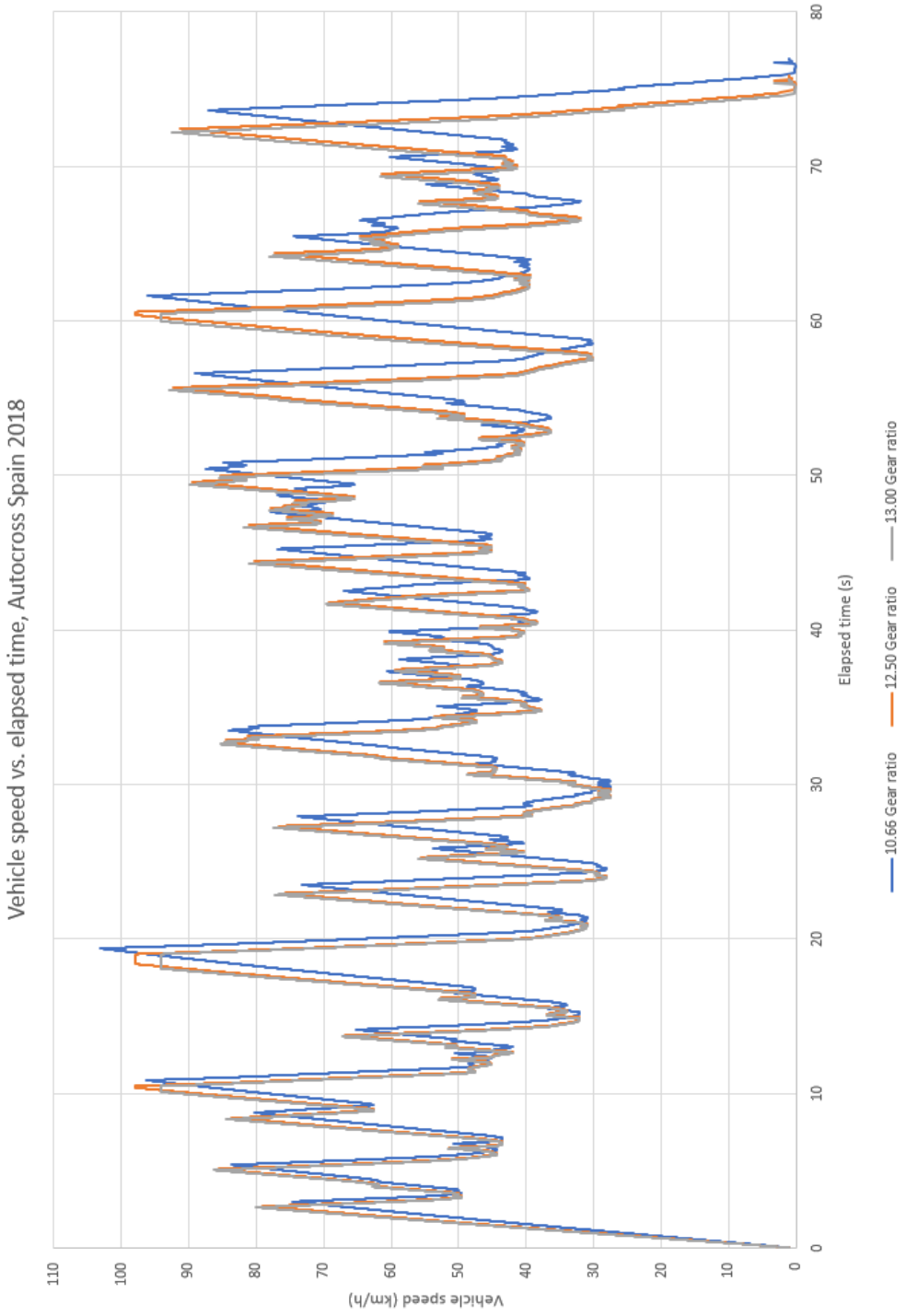

Appendix 2 – Spreadsheet for mass of drivetrain assembly

System mass	*Mass (kg)*
Transmission unit	1,7
Motor unit	4,0
Drivetrain assembly	5,7
Drivetrain assembly x4	22,7
HPF019 drivetrain	47,5
Difference	52 %

Motor unit breakdown	*Mass (kg)*
Motor unit components	1,10
Stator (measured in real life)	2,42
Rotor (measured in real life)	0,33
Encoder (datasheet)	0,13

Accounting for hubs + uprights	*Mass (kg)*
Front upright (suggested)	0,57
Front upright (HPF019)	0,44
Front upright difference	0,13
Wheel hub (suggested)	0,46
Front wheel hub (HPF019)	0,34
Rear wheel hub (HPF019)	0,48
HPF019 wheel hubs (2F+2R)	1,64
Suggested wheel hubs x4	1,85
Difference in suggested&HPF019	0,21
As above but /4	0,05
Transmission unit, no upright, no hub	0,71
As above but plus hub&upright difference	0,89
Above x4 + motor unit x4	19,49
difference to 19	58,98 %

Compensated system mass	*Mass (kg)*
Transmission unit	0,9
Motor unit	4,0
Drivetrain assembly	4,9
Drivetrain assembly x4	19,5
HPF019 drivetrain	47,5
Difference	59 %